# Copy-Number Variation Contributes to the Mutational Load of Bardet-Biedl Syndrome

Anna Lindstrand,[1,9] Stephan Frangakis,[1] Claudia M.B. Carvalho,[2,3] Ellen B. Richardson,[1] Kelsey A. McFadden,[1] Jason R. Willer,[1] Davut Pehlivan,[2] Pengfei Liu,[2] Igor L. Pediaditakis,[1] Aniko Sabo,[2,4] Richard Alan Lewis,[2,5] Eyal Banin,[6] James R. Lupski,[2,4,7,8] Erica E. Davis,[1,*] and Nicholas Katsanis[1,*]

Bardet-Biedl syndrome (BBS) is a defining ciliopathy, notable for extensive allelic and genetic heterogeneity, almost all of which has been identified through sequencing. Recent data have suggested that copy-number variants (CNVs) also contribute to BBS. We used a custom oligonucleotide array comparative genomic hybridization (aCGH) covering 20 genes that encode intraflagellar transport (IFT) components and 74 ciliopathy loci to screen 92 unrelated individuals with BBS, irrespective of their known mutational burden. We identified 17 individuals with exon-disruptive CNVs (18.5%), including 13 different deletions in eight BBS genes (*BBS1*, *BBS2*, *ARL6/BBS3*, *BBS4*, *BBS5*, *BBS7*, *BBS9*, and *NPHP1*) and a deletion and a duplication in other ciliopathy-associated genes (*ALMS1* and *NPHP4*, respectively). By contrast, we found a single heterozygous exon-disruptive event in a BBS-associated gene (*BBS9*) in 229 control subjects. Superimposing these data with resequencing revealed CNVs to (1) be sufficient to cause disease, (2) Mendelize heterozygous deleterious alleles, and (3) contribute oligogenic alleles by combining point mutations and exonic CNVs in multiple genes. Finally, we report a deletion and a splice site mutation in *IFT74*, inherited under a recessive paradigm, defining a candidate BBS locus. Our data suggest that CNVs contribute pathogenic alleles to a substantial fraction of BBS-affected individuals and highlight how either deletions or point mutations in discrete splice isoforms can induce hypomorphic mutations in genes otherwise intolerant to deleterious variation. Our data also suggest that CNV analyses and resequencing studies unbiased for previous mutational burden is necessary to delineate the complexity of disease architecture.

## Introduction

Bardet-Biedl syndrome (BBS [MIM: 209900]) is a rare (1:13,500–1:160,000) multisystemic developmental disorder characterized by retinal dystrophy, obesity, polydactyly, intellectual disability, renal dysfunction, and hypogonadism. During the past 15 years, causal variants in 21 different genes have been identified,[1–22] and in vivo and in vitro studies have established the cellular basis of BBS as a defect of ciliary function.[2] Biochemical characterization of the cilium has shown that it is composed of at least four different functional complexes: the BBSome, the transition zone, and two intraflagellar transport complexes.[23] BBS proteins are thought to localize mainly to the BBSome and the transition zone,[24] with the exception of recent reports of pathogenic mutations in *IFT27* (MIM: 6158700)[1] and *IFT172* (MIM: 607386)[22] encoding components of IFT complex B, that localize primarily to cilia. Furthermore, some BBS genes have also been linked to other ciliopathies, including Meckel-Gruber syndrome (MKS [MIM: 249000]), Joubert syndrome (JBTS [MIM: 213300]), Senior-Løken syndrome (SLS [MIM: 266900]), nephronophthisis (NPHP [MIM: 256100]), and Leber congenital amaurosis (LCA [MIM: 204000]), illustrating the genetic, biological, and clinical overlap within these genetic disorders.[9,25–28] Alström syndrome (ALMS [MIM: 203800]), caused by mutations in *ALMS1* (MIM: 606844), overlaps clinically with BBS, sharing common characteristics such as obesity, diabetes, and retinal dystrophy.[29,30]

Although BBS is viewed traditionally as an autosomal-recessive Mendelian trait, oligogenic inheritance has been documented for most BBS-associated genes. In rare cases, at least one deleterious (typically heterozygous) allele in a different BBS-associated gene modifies the penetrance of the disorder.[2,30–34] More commonly, *trans* modifier alleles contribute to variable expressivity, not only in BBS, but across the ciliopathy spectrum.[35,36] For example, a common c.685G>A (p.Ala229Thr) mutation in *RPGRIP1L* (MIM: 610937) is associated with retinitis pigmentosa in ciliopathies;[36] similarly, nephronophthisis-affected individuals with a homozygous *NPHP1* (MIM: 607100) deletion are more likely to develop retinal degeneration if they also bear the AHI1 p.Arg830Trp variant in the heterozygous state.[37] Moreover, resequencing across different ciliopathy cohorts unbiased for known mutations has demonstrated an enrichment of deleterious heterozygous changes in *TTC21B* (MIM: 612014), a key component of the retrograde IFT machinery, in affected individuals versus control subjects.[35] These data have created a model in which, in addition to primary causal alleles, the

[1]Center for Human Disease Modeling, Duke University School of Medicine, Durham, NC 27701, USA; [2]Department of Molecular and Human Genetics, Baylor College of Medicine, Houston, TX 77030, USA; [3]Centro de Pesquisas René Rachou – FIOCRUZ, Belo Horizonte, MG 30190-002, Brazil; [4]Human Genome Sequencing Center, Baylor College of Medicine, Houston, TX 77030, USA; [5]Department of Ophthalmology, Baylor College of Medicine, Houston, TX 77030, USA; [6]Center for Retinal and Macular Degenerations, Department of Ophthalmology, Hadassah-Hebrew University Medical Center, Jerusalem 91120, Israel; [7]Department of Pediatrics, Baylor College of Medicine, Houston, TX 77030, USA; [8]Texas Children's Hospital, Houston, TX 77030, USA
[9]Present address: Department of Molecular Medicine & Surgery, Karolinska Institutet, 17176 Stockholm, Sweden
*Correspondence: erica.davis@duke.edu (E.E.D.), katsanis@cellbio.duke.edu (N.K.)
http://dx.doi.org/10.1016/j.ajhg.2015.04.023.
© 2016 American Society of Human Genetics.

mutational burden or "load" in the ciliary proteome, defined as the total number, mutational type, and locus distribution of deleterious alleles, has a role in defining disease presentation, especially the elaboration of endophenotypes.[23] Notably, *trans* modifying alleles can be deleterious or protective, as evidenced by the ability of homozygous loss-of-function *Mkks/Bbs6* alleles to ameliorate retinal degeneration in a *Cep290* mouse model,[38] as well as the postulated protective effect of *CEP290* (MIM: 610142) haploinsufficiency in the context of de novo deletions in 16p11.2 (MIM: 611913) that are associated with complex neurocognitive traits.[39]

In the past decade, copy-number variants (CNVs) have emerged as major contributors to the genetic burden of both rare and common disorders.[40] A number of CNVs have been associated with human genomic disorders, such as microdeletion and duplication syndromes,[41,42] as well as dose changes involving single loci[43,44] and recessive carrier states.[45] In BBS, CNVs have been reported episodically.[46,47] More recently, we have shown that the 290 kb recurrent deletion of *NPHP1*, usually underlying renal ciliopathies including NPHP[48,49] and SLS,[50] is both a likely driver (primary causal locus under a recessive paradigm) of BBS in one family and is also enriched in BBS-affected case subjects.[11] These observations prompted us to investigate systematically whether CNVs contribute to mutational load in BBS. Here, through high-resolution analysis of bona fide genes involved in BBS, other ciliopathies, and/or core ciliary components, we report exon-disruptive CNVs in 18.5% of unrelated BBS-affected individuals, most of which are driven by recombination at intronic repetitive elements. When combined with sequencing data from all assayed loci, our analyses indicate that (1) these events can represent recessive mutational drivers, with homozygous exonic or whole gene deletions; (2) they can Mendelize heterozygous deleterious variants; and (3) they can unmask genetic interactions with recessive mutations in other BBS genes. When combined with in vivo modeling of likely pathogenic SNVs, our observations improve the resolution of BBS-associated gene contribution to disease; support further a mutational burden model that includes distinct classes of variant alleles (SNV plus CNV); facilitate the identification of candidate loci through a mutational mechanism that involves the ablation of a specific splice isoform; and illuminate further the genetic complexity of this disorder.

## Subjects and Methods

### Research Participants

A total of 92 unrelated BBS-affected individuals and 229 non-BBS control subjects were analyzed by aCGH. Affected individuals were selected irrespective of previously identified pathogenic changes. The control samples included 137 individuals of northern European descent from our Age Related Macular Degeneration control cohort,[51,52] five HapMap samples of western European ancestry, and anonymized samples from 87 healthy internal lab control subjects of northern European descent. We used standard methods to isolate genomic DNA from peripheral blood. Informed consent was obtained from all participating individuals, with approval from the Institutional Review Boards of the Duke University Medical Center and the Baylor College of Medicine.

### Whole-Genome Amplification

30 ng of genomic DNA from affected participants and gender-matched male (NA10851) and female (NA15510) control DNAs (obtained from Coriell Cell Repositories) were amplified by whole-genome amplification (GenomePlex Whole Genome Amplification Kit, Sigma). Amplified product was verified by gel electrophoresis and quantified by UV absorbance at 260 nm with a NanoDrop (ND-1000) spectrophotometer (NanoDrop Technologies).

### Oligonucleotide aCGH Analyses

We used a 4×180k array format at an average coverage of one probe per 100 base pairs (bp) in coding sequences and one probe per 500 bp in intragenic non-coding sequences. The high-resolution targeted aCGH design was created in Agilent's web portal eArray and slides were ordered from Agilent Technologies. In brief, 2 μg of each amplified BBS DNA sample and 1.2 μg of unamplified control DNA sample were then labeled and hybridized as described.[53]

### Junction Sequence Analyses

Long-range PCR was conducted with the Phusion High-Fidelity PCR Kit (NEB, E0553L) according to the manufacturer's protocol, and PCR products that were unique to carriers and not observed in control subjects were Sanger sequenced.

### Quantitative PCR Confirmation of CNVs

When junction fragments failed to amplify by multiple primer pairs, we used quantitative (q)PCR to confirm CNVs. TaqMan Copy Number Assays (Life Technologies) were selected from within the CNV regions. We conducted triplicate reactions according to an ABI protocol on an ABI7900HT Fast Real-Time PCR System for both case subjects and matched control subjects. A copy neutral reference assay was performed in parallel (RNase P) for normalization purposes. Data were analyzed and visualized with CopyCaller (v.1.0).

### Resequencing of BBS Genes

We amplified all exons and splice junctions of *BBS1* (MIM: 2099010), *BBS2* (MIM: 6061510), *ARL6/BBS3* (MIM: 608845), *BBS4* (MIM: 600374), *BBS5* (MIM: 603650), *MKKS/BBS6* (MIM: 604896), *BBS7* (MIM: 607590), *TTC8/BBS8* (MIM: 608132), *BBS9* (MIM: 607968), *BBS10* (MIM: 610148), *TRIM32/BBS11* (MIM: 602290), *BBS12* (MIM: 610683), *MKS1/BBS13* (MIM: 609883), *CEP290/BBS14* (MIM: 609883), *WDPCP/BBS15* (MIM: 613580), *SDCCAG8/BBS16* (MIM: 613524), *IFT27/BBS19*, and *NPHP1* in the 17 individuals harboring CNVs, and we conducted bidirectional Sanger sequencing on an ABI3730 according to standard protocols. Identified mutations were segregated by Sanger sequencing in all available family members. Variants (CNVs or SNVs) were named according to the following NCBI GenBank reference transcript accession numbers: *BBS1*, NM_024649.4; *BBS2*, NM_031885.3; *ARL/BBS3*, NM_032146.4; *BBS4*, NM_033028.4; *BBS5*, NM_152384.2; *MKKS/BBS6*, NM_018848.3; *BBS7*, NM_176824.2; *TTC8/BBS8*, NM_144596.3;

*BBS9*, NM_198428.2; *BBS10*, NM_024685.3; *ALMS1*, NM_015120.4; *CEP290*, NM_025114.3; *SDCCAG8*, NM_006642.3; *NPHP1*, NM_000272.3; *IFT74*, NM_025103.2.

### Transient Gene Suppression in Zebrafish Embryos

All zebrafish studies were approved by the Duke University Institutional Animal Care and Use Committee. Translation-blocking and splice-blocking morpholino (MO) antisense oligonucleotides were designed by and obtained from Gene Tools. To determine the optimal dose for in vivo complementation assays and genetic interaction studies, we injected increasing doses of MO into 1- to 4-cell-stage wild-type (WT) zebrafish embryos. To determine MO efficiency (splice-blocking MOs), we harvested injected embryos in Trizol (Invitrogen), extracted total RNA according to the manufacturer's instructions, and generated oligo-dT-primed cDNA with the QuantiTect reverse transcription kit (QIAGEN) for use as a template for RT-PCR; subsequent Sanger sequencing of RT-PCR products identified the precise alteration of endogenous transcript.

### In Vivo Complementation and Genetic Interaction Studies in Zebrafish

For rescue experiments, human *IFT74* (MIM: 608040) transcript variant 1 (long; GenBank: NM_025103.2) and *IFT74* transcript variant 2 (short; NM_001099224.1) messages were amplified from cDNA generated from a human fibroblast cell line; *SDCCAG8* (NM_006642.3; clone T8331) was obtained commercially (Genecopoeia); and all ORFs were subcloned into the pCS2+ vector and transcribed in vitro via the mMessageMachine kit (Ambion). All other BBS gene ORF clones and mutagenesis procedures have been described.[9,11,54] For genetic interaction studies, subeffective doses of MO (producing <30% affected embryos/batch when injected alone) were injected in single, pairwise, or triple combinations to assess additive or epistatic effects.

### qPCR to Monitor Endogenous *bbs* Gene Expression

We harvested embryo batches (n = 20 embryos/batch) at the mid-somite stage in Trizol (Invitrogen), extracted total RNA, and generated oligo-dT-primed cDNA with the QuantiTect reverse transcription kit (QIAGEN) for use as a template for RT-PCR (30 ng template/reaction). We used SYBR Green PCR Master Mix (ThermoFisher) to monitor gene expression profiles in real-time on an ABI7900HT instrument, and cycle threshold (Ct) values were computed with SDS 2.3 software (Applied Biosystems) according to manufacturer's instructions. All experiments were conducted in triplicate wells corresponding to each gene with at least one biological replicate. Mean Ct values for reference genes (*acta1b* [GenBank: NM_214784.2], *actb1* [NM_131031.1], or *actb2* [NM_181601.4]) were used to normalize mean Ct values for test genes (*bbs2* [NM_152887.1], *bbs4* [NM_001077466.2], *mkks/bbs6* [NM_200165.1], *bbs5* [NM_200299.1], and *bbs10* [NM_001089463.1]) and Kruskal-Wallis tests were used to compare differences between experimental conditions. Primer sequences are available upon request.

### CRISPR/CAS9 Genome Editing of *ift74*

We used the CRISPR Design tool to identify *ift74* (GenBank: NM_001002385.1) guide (g)RNA target sequences, for which two oligonucleotides were synthesized and annealed. Annealed oligos were then ligated into the T7cas9sgRNA2 vector as described,[55] and plasmids prepped from individual clones were sequence confirmed. Template vector was linearized with BamHI and gRNA was transcribed using the MEGAshortscript T7 kit (Life Technologies). A total of 50 pg of *ift74* gRNA and 200 pg of CAS9 protein (PNA Bio) was co-injected into individual cells of 1-cell-stage embryos. To determine targeting efficiency in F0 mutants, we harvested single embryos in Trizol (Invitrogen) at 2 dpf (three controls and eight F0 mutants), extracted total RNA according to manufacturer's instructions, reverse transcribed cDNA using the QuantiTect reverse transcription kit (QIAGEN), and PCR amplified a region flanking the gRNA target site. PCR products were denatured, reannealed slowly, and separated on a 15% TBE 1.0 mm precast polyacrylamide gel (BioRad) as described.[56] The resulting PAGE gel was incubated in ethidium bromide and imaged on a Biorad ChemiDoc system. To estimate the percent mosaicism, RT-PCR products were gel purified (QIAGEN) and cloned into a TOPO-TA vector (ThermoFisher). Plasmid was prepped from multiple individual colonies per embryo (n = 8–15) and Sanger sequenced on an ABI3730 instrument according to standard protocols.

### Phenotypic Analyses in Zebrafish

Embryo batches were assessed live at the 8- to 10-somite stage for early developmental defects in gastrulation (shortened body axis, widened and kinked notochord, and widened and thinned somites) and were categorized into class I (moderately affected) or class II (severely affected) according to previously established objective criteria.[9,11,20,21,35,36,54] Live embryo images were acquired on a Nikon AZ100 microscope at 8× magnification facilitated by NIS Elements software and statistical comparisons were conducted with $\chi^2$ tests. Renal structure was assessed in *bbs* or ciliopathy gene models as described.[11,57] In brief, larvae were fixed in Dent's solution at 4 days post fertilization (dpf) and immunostained with anti-$Na^+/K^+$ ATPase antibody (a6F, Developmental Studies Hybridoma Bank) to demarcate renal tubules. Larvae were imaged on a Nikon AZ100 microscope at 4× magnification facilitated by NIS Elements software; renal structures (area of the proximal convoluted tubule, or tubule diameter adjacent to the proximal convoluted tubule) were measured with ImageJ software (NIH); statistical comparisons were conducted with a Student's t test.

## Results

### Identification of Intragenic CNVs in BBS

To evaluate the contribution of CNVs to BBS, we investigated a cohort of 92 unrelated BBS-affected individuals (Table 1), without preselection based on known mutation status. To improve the accuracy of CNV detection and to achieve sub-kb resolution, we focused on a genetically and biologically plausible preselected set of genes. We therefore generated a custom high-resolution oligonucleotide aCGH targeting of a total of 94 genes. These included the 17 known BBS genes (at the time of the design of the array); 20 genes encoding components of the IFT complex; and 57 additional loci associated with ciliopathies (Table S1). With this defined gene set, we designed probes at a density of one probe per 100 bp of coding sequence and one probe per 500 bp in intragenic regions.

In addition to the previously reported recurrent deletion at the *NPHP1* locus (found in one homozygous and two

**Table 1. Clinical Phenotype Summary of BBS-Affected Case Subjects with CNVs**

| Individual | Primary Locus | Consanguinity | Sex | Age | RP | Ob | PD | HG | RD | ID | DD | Others |
|---|---|---|---|---|---|---|---|---|---|---|---|---|
| AR240-03 | *BBS1* | – | F | 21 | ✓ | ✓ | ✓ | ND | – | ✓ | – | S, OM |
| AR246-03 | *BBS1* | – | M | 12 | ✓ | ✓ | ✓ | ✓ | – | ✓ | ✓ | M, DC, MT, E |
| AR380-03 | *BBS1* | – | F | 9 | ✓ | ✓ | ✓ | ND | – | ✓ | – | PS, OM, H |
| AR888-03[11] | *BBS1* | – | M | 4 | ✓ | ✓ | ✓ | ND | ✓ | ✓ | ✓ | OM, S, HL, Ns, Sz, SA |
| KK047-05 | *BBS2* | ✓ | M | 9 | ✓ | ✓ | ✓ | ✓ | ND | ✓ | ND | |
| KK11-04 | *ARL6/BBS3* | ✓ | M | 17 | ✓ | ✓ | ✓ | ✓ | ND | ND | ✓ | Hs, UT |
| KK11-09 | *ARL6/BBS3* | ✓ | F | 7 months | ND | ND | ✓ | ND | ND | ND | ND | |
| DM034-004 | *ARL6/BBS3* | – | M | 10 | ✓ | ✓ | ✓ | ND | ND | – | – | As, DM1, FL |
| 32/3 | *BBS4* | – | M | 8 | ✓ | ND | ND | ND | ND | ND | ND | |
| AR800-03 | *BBS4* | – | M | 5 | ✓ | ✓ | ✓ | ✓ | ND | ✓ | ND | St, SS, F |
| AR400-03 | *BBS4* | – | F | 11 | ✓ | ✓ | ✓ | ND | ND | ✓ | ✓ | A, M, As, OM, UH, ST |
| AR634-03 | *BBS7* | – | F | 17 | ✓ | ✓ | – | ND | – | ✓ | ✓ | M, As, DM2 |
| AR634-04 | *BBS7* | – | M | 15 | ✓ | ✓ | – | ✓ | ND | ✓ | ND | M, AS, HL |
| 44/3[11] | *BBS7* | – | M | | ✓ | ✓ | ✓ | ✓ | ✓ | ND | ✓ | |
| AR883-04 | *BBS10* | – | M | 4 | ✓ | ✓ | ✓ | ND | ✓ | ✓ | ND | SA, Sz, OM |
| AR672-04 | *IFT74* | – | M | 36 | ✓ | ✓ | ✓ | ✓ | – | ✓ | – | MC |
| RC2-03[11] | *NPHP1* | ✓ | M | 6 | ✓ | – | ✓ | ✓ | ✓ | ND | ✓ | Ns, F |
| AR811-03 | unknown | ✓ | M | 4 | ✓ | ✓ | ND | ✓ | ND | ND | ✓ | SA |
| AR704-03[11] | unknown | – | F | | ✓ | ✓ | ✓ | ND | ND | ✓ | ND | |

Phenotypes are indicated as present (✓) or absent (–). Age at assessment is indicated in years, unless otherwise noted. ND indicates no data because subject was not evaluated. Phenotypes assessed: RP, retinitis pigmentosa; Ob, obesity; PD, polydactyly; HG, hypogonadism; ID, intellectual disability; RD, renal disease; DD, developmental delay. Others: MC, microcephaly; M, myopia; S, scoliosis; OM, otitis media; DM1, diabetes mellitus type 1; DM2, diabetes mellitus type 2; HL, hearing loss; DC, dental crowding; MT, missing teeth; E, eczema; PS, pulmonary stenosis; H, hypertension; Ns, nystagmus; Sz, seizures; St; strabismus; SS, short stature; A, asthma; UH, umbilical hernia; ST, sickle trait; As, astigmatism; FL, fatty liver; F, farsighted; SA, sleep apnea; Hs, hypospadias; UT, undescended testis.

heterozygous BBS-affected individuals) and a 17 kb heterozygous deletion in *BBS1* identified in the same cohort,[11] we detected another 14 unique intragenic CNVs in 13 individuals with BBS: 13 deletions (ranging in size from 730 bp to 172 kb) and 1 complex intragenic duplication (Tables 1, 2, and 3; Figures 1, 2, and S1). These data, combined with our recent report,[11] total 16 different CNVs among 17 unrelated individuals from the same BBS cohort.

### Breakpoint Analysis Shows Multiple Mechanisms of CNV Formation

To refine CNV endpoints, to map precisely the genomic content, and to examine rearrangement end products as a means of inferring possible underlying formation mechanisms, we characterized 13 of 15 non-recurrent breakpoint junctions by long-range PCR and Sanger sequencing (Table 3; Figure S1).[11] None of the 15 CNVs detected by high-resolution aCGH in the BBS genes (*BBS1*, *BBS2*, *ARL6/BBS3*, *BBS4*, *BBS5*, *BBS7*), *ALMS1*, *IFT74*, and *NPHP4* in our cohort have been reported previously or are present in the Database of Genomic Variants (DGV), except for the heterozygous deletion in *BBS1* (AR888-03) that we published recently[11] and a *BBS5* deletion of similar size and position to individual 32/3 that has been found (in heterozygosity) in two database entries: one subject with reported developmental delay and one with obesity. We found three individuals with unique CNVs in *BBS4*; two of them involve exons 5–6 as determined by breakpoint mapping. Remarkably, individuals with deletions and differing breakpoints in *BBS4* involving the same exons have been reported,[13,47] suggesting that this region might be susceptible to genomic instability (Tables 2 and 3; Figure 1).

In 6 of 15 (40%) non-recurrent CNVs (AR888-03, *BBS1*; AR246-03, *BBS1*; 32/3, *BBS4*; AR400-03, *BBS4*; AR883-04, *BBS5*; AR672-04, *IFT74*), the junctions were located within *Alu* elements with variable percentage of sequence identity (77%–92%), suggesting that the deletions were mediated by *Alu-Alu* recombination. *Alu-Alu* recombination forming an *Alu* hybrid is a prominent mechanism underlying the formation of pathogenic CNVs associated with distinct diseases.[58–62] In two junctions, substrate pairs of *Alu* repeats from the same family (AR888-03, *AluY-AluY*; AR246-03, *AluSp-AluSp*) are involved whereas the remaining four have substrate pairs consisting of distinct *Alu* repeat families mediating CNV formation (32/3, *AluSc8* - *AluSx*; AR400-03, *AluSx* - *AluSg*; AR883-04, *AluYc3* - *AluSg*; AR672-04, *AluSx* - *AluY*). Notably, a particular *AluSx* is

present at the proximal junction of non-recurrent *BBS4* deletions present in two unrelated BBS-affected individuals (AR400-03 and 32/3). In addition, a simple dinucleotide microsatellite repeat, (TG)n, 4 kb apart and consisting of 41 nt, seems to be involved in the formation of the CNV in individual KK11-04 (*ARL6/BBS3*).

The formation of complex rearrangements such as triplications and inversions mediated by *Alu-Alu* recombination and the co-occurrence of point mutations and indels at or near the CNV breakpoint junctions implicate replication-based mechanisms (RBMs),[63,64] but simple rearrangements may be caused by double-strand breaks repaired by single-strand annealing (SSA) by the sequence similarity for annealing the broken DNA.[65] In two *Alu-Alu*-mediated CNVs, additional point mutations were observed: a T>C SNV 178 bp from the junction of *BBS1* in AR888-03[11] and a deletion of nine nucleotides in a poly(A) region involved in the formation of the breakpoint junction of *IFT74* in AR672-04 (Figure 3), potentially implicating an error-prone DNA polymerase and a RBM underlying formation of those variants. Because those CNVs are inherited, we could not confirm whether the SNVs and the rearrangement were formed concomitantly.

Six additional deletion CNVs presented with no homology, 1 to 5 bp homology, or 5 bp nucleotide insertions at the breakpoint junctions (Table 3; Figures 1 and S1), indicative of canonical non-homologous end joining (NHEJ), microhomology-mediated end joining (MMEJ),[66] or RBM as underlying mechanisms. Of note, breakpoint junctions of CNVs spanning *ALMS1* (AR400-03) and *BBS7* (AR634-03) presented five base pair insertions (Table 3; Figure S1) that could have originated from within the deleted region as a templated insertion (indicating either RBM or MMEJ); nonetheless, the short length of such insertions makes it difficult to rule out random bp insertion that can also occur during NHEJ.

In two cases we were unable to obtain junction fragments, and therefore confirmed the aberrations with TaqMan Copy Number Assays; both CNVs, the 14.9 kb *BBS1* deletion (individual AR240-03) and the complex duplication in *NPHP4* (MIM: 607215; individual AR811-03), displayed the expected dosage alteration (Figure S1).

### Enrichment of Ciliary Gene CNVs in BBS-Affected Case Subjects

Subsequent to breakpoint analysis and CNV confirmation, we asked whether there was an increased prevalence of CNVs within our target ciliary gene set in BBS-affected case subjects. A search in the DGV revealed a single heterozygous CNV in *BBS5* (9969)[67] overlapping with those identified in our BBS cohort; the CNV was of similar size and genomic location as the deletion detected in AR883-04. However, mindful of likely resolution differences between CNVs in this database and our study, we performed aCGH with the same reagent, hardware, and analytic software on 229 healthy control individuals. We did not detect any of the discovered CNVs in these controls; analysis for any exon-disrupting CNV identified a sole heterozygous deletion of exons 5–7 of *BBS9*, predicted to result in an in-frame deletion of 133 amino acids. These data, together with our previously reported *NPHP1* and *BBS1* CNVs,[11] suggest an incidence of exon-disruptive CNVs at 13.6% (25/184) of BBS chromosomes compared to 0.2% (1/458) of control chromosomes, respectively, constituting a significant enrichment ($p < 0.0001$, Fisher's exact test).

### BBS-Associated Gene CNVs Contribute Recessive Alleles

Next, we investigated how the CNVs disrupting BBS-associated genes contribute to disease manifestation. For cases in which parental samples were available (13 of 17), segregation analysis showed all CNVs to be inherited (Table 2; Figure 2).[11] Among the six BBS-affected pedigrees harboring non-recurrent homozygous deletions, familial DNAs segregated according to Mendelian expectations, demonstrating anticipated carrier status for both parents in three pedigrees (AR800, DM034, KK11) and a single carrier parent in two pedigrees (KK47 and AR400; DNA was unavailable for the other parent; Figure 2). Five of six pedigrees had only a single affected individual. Nonetheless, the nature of the gene disruptive deletion, ranging from two to eight exons, suggested strongly that these CNVs are likely BBS drivers. For KK47, AR800, and AR400, the putative splicing of exons flanking the deletions is predicted to result in a frameshift and premature termination codon. In DM034, the six exons encoding the C-terminal end of *ARL6/BBS3* are deleted, predicted to result in a 41 amino acid truncated protein bereft of the majority of the ADP-ribosylation factor domain. Affected individual 32/3 harbored a two-exon deletion that would not alter the reading frame if spliced, but would delete part of the first tetratricopeptide (TPR) domain in BBS4, known to be important for protein-protein interactions.[68] Finally, deletion of a single exon in Saudi pedigree KK11 is predicted to result in truncation of 23 amino acids from the C-terminal end of ARL6/BBS3; the presence of the same homozygous exon 8 deletion in affected sibling KK11-09 bolstered our confidence in the pathogenicity of this CNV as the primary driver of disease.

Unmasking a recessive allele on one chromosome by a deletion on the other is a recognized disease-causing mechanism.[69–72] For BBS, we reported previously that this phenomenon contributes to pathology in a *BBS1* pedigree.[11] Consistent with this observation, segregation analysis of a previously reported[73] maternally inherited *BBS7* c.878A>C (p.Gln293Pro) change in AR634 showed this variant to be in *trans* with the paternally inherited exon 16–17 deletion; both affected siblings carried the two *BBS7* alleles (Figure 2; Table S2). To determine whether this mechanism could explain disease in any of the three pedigrees with heterozygous *BBS1* deletions, we sequenced the coding exons and splice junctions in each of AR240, AR246, and AR380. In each case, we identified the c.1169T>G (p.Met390Arg) mutation, known to be one of

**Table 2. Mutational Findings of 17 Individuals Affected with BBS Harboring CNVs Encompassing BBS Genes**

| Sample ID | Primary Causal Locus | Allele 1 | Allele 2 | Additional Mutational Burden | Genotype Counts in 6,503 Controls (EVS All) | In Vivo Pathogenicity Score |
|---|---|---|---|---|---|---|
| **Primary Causal Locus: Homozygous CNV** | | | | | | |
| KK047-05 | *BBS2* | del: exon8_15 (pat)[a,b] | del: exon8_15 (mat)[b] | none | NA | NA |
| DM034-004 | *ARL6/BBS3* | del: exon4_9 (pat)[b] | del: exon4_9 (mat)[b] | none | NA | NA |
| KK11-04 | *ARL6/BBS3* | del: exon8 (pat)[b] | del: exon8 (mat)[b] | *SDCCAG8*: c.1594G>A (p.Glu532Lys) het (mat) | 0 | hypomorph |
| 32/3 | *BBS4* | del: exon3_4 (U)[b] | del: exon3_4 (U)[b] | none | NA | NA |
| AR800-03 | *BBS4* | del: exon5_6 (pat)[b] | del: exon5_6 (mat)[b] | *MKKS/BBS6*: c.724G>T (p.Ala242Ser) het[73] | AA = 0, AC = 58, CC = 6,445 | dominant-negative[54] |
| | | | | *BBS2*: c.367A > G (p.Ile123Val) hom (Pat, Mat) | CC = 240, CT = 2,060, TT = 4,198 | hypomorph[54] |
| AR400-03 | *BBS4* | del: exon5_6 (pat)[a,b] | del: exon5_6 (mat)[b] | *BBS9* c.1993C>T (p.Leu665Phe) het (pat)[a] | TT = 0, TC = 42, CC = 6,461 | null |
| | | | | *ALMS1* del exon16_17 het (pat)[a,b] | NA | NA |
| RC2-03[11] | *NPHP1* | del: whole gene (pat)[b] | del: whole gene (mat)[b] | *BBS2*: c.367A>G (p.Ile123Val) hom (pat, mat) | CC = 240, CT = 2,060, TT = 4,198 | hypomorph[54] |
| **Primary Causal Locus: Compound Heterozygous CNV + SNV** | | | | | | |
| AR380-03 | *BBS1* | del: exon9_12 (U)[b] | c.1169T>G (p.Met390Arg) (U); (rs113624356) | none | NA | NA |
| AR888-03[11] | *BBS1* | del: exon1_11 (pat)[b] | c.1645G>T (p.Glu549*) (mat); (rs121917777) | *NPHP1*: c.14G>T (p.Arg5Leu) het (mat) | AA = 0, AC = 6, CC = 6,497 | hypomorph[11] |
| | | | | *BBS4*: c.439T>A (p.Tyr147Asn) het (pat) | 0 | null |
| | | | | *BBS5*: c.584A > G (p.Asp195Gly) het (mat) | GG = 0, GA = 4, AA = 6,497 | null |
| | | | | *BBS7*: c.442A>C (p.Asn148His) het (mat) | 0 | null |
| AR240-03 | *BBS1* | del: exon10_17 (mat)[b] | c.1169T>G (p.Met390Arg) (pat); (rs113624356) | *BBS5*: c.551A>G (p.Asn184Ser) het (mat) | GG = 0, GA = 61, AA = 6,440 | null[54] |
| AR246-03 | *BBS1* | del: exon14_17 (U)[b] | c.1169T>G (p.Met390Arg) (U); (rs113624356) | *BBS10*: c.2119_2120delGT (p.Val707*) het (U)[20] | 0 | ND |
| AR634-03 | *BBS7* | del: exon16_17 (pat)[b] | c.878A>C (p.Gln293Pro) (mat) | *BBS4*: c.137A>G (p.Lys46Arg) het (mat) | GG = 0, GA = 92, AA = 6,403 | null[54] |
| | | | | *IFT74*: c.1735G>A (p.Val579Met) het (U) | AA = 0, AG = 97, GG = 5,884 | benign |
| AR672-04 | *IFT74* | del: exon14_19 (mat)[b] | c.1685–1G>T (pat); (rs200699377) | none | NA | NA |

(*Continued on next page*)

**Table 2.** *Continued*

| Sample ID | Primary Causal Locus | Allele 1 | Allele 2 | Additional Mutational Burden | Genotype Counts in 6,503 Controls (EVS All) | In Vivo Pathogenicity Score |
|---|---|---|---|---|---|---|
| **Heterozygous CNV Contributes Additional Mutational Burden** | | | | | | |
| AR883-04 | *BBS10* | c.2119_2120delGT (p.Val707*) (pat) | c.2118_2119delTG (p.Val707fs*) (mat) | *BBS5*: del: exon8_12 het (mat)[b] | NA | NA |
| 44/3[11] | *BBS7* | c.87_88delCA (p.His29Glnfs*12) (pat) | c.87_88delCA (p.His29Glnfs*12) (mat) | *NPHP1*: del whole gene het (mat)[b] | NA | NA |
| | | | | *CEP290* c.6727G>C (p.Glu2243Gln); c.6401T>C (p.Ile2134Thr) het (mat) | 0; GG = 0, GA = 64, AA = 5,768 | hypomorph |
| AR704-03[11] | unknown | NA | NA | *NPHP1*: del whole gene het (mat)[b] | NA | NA |
| | | | | *BBS10*: c.145C>T (p.Arg49Trp) het (pat) | 0 | null[54] |
| | | | | *TTC8/BBS8*: c.1253A>G (p.Gln418Arg) het (mat) | GG = 0, GA = 27, AA = 6,476 | hypomorph |
| AR811-03 | unknown | NA | NA | *NPHP4*: het dup exon1_28; normal exon29; het dup exon 30 (U)[b] | NA | NA |

Abbreviations are as follows: pat, paternal; mat, maternal; U, unknown inheritance; hom, homozygous; het, heterozygous; del, deletion; dup, duplication; EVS, Exome Variant Server; NA, not applicable; ND, no data.
[a]No DNA available from the father, deletion detected in the grandfather.
[b]CNVs.

the two most frequently mutated sites among BBS loci and a known hypomorphic allele,[14,54,74,75] in *trans* with the deletion and segregating according to Mendelian expectations with disease in each pedigree (Figure 2; Tables 2 and S2). Notably, Sanger sequencing of *BBS1* exon 12 in AR380-03 showed c.1169T>G as an apparently homozygous mutation because the encompassing deletion masks the zygosity of the change. Sanger sequencing of *BBS5* by a similar strategy in AR883, a pedigree carrying a heterozygous exon 8–12 deletion, yielded no additional functional variants in *BBS5*. Together, the presence of either a homozygous gene deletion (n = 7) or a heterozygous deletion in *trans* with a pathogenic SNV in the same gene (n = 5) assigned a primary genetic cause for a previously underappreciated proportion of our cohort (13%; Figure 2).[11]

### *IFT74*, a BBS Candidate Gene

Next, we asked whether CNV deletions could assist in the identification of BBS genetic drivers. Among the families studied, there was a single individual, AR672-04, who was bereft of known driver mutations, but harbored a heterozygous deletion CNV. Our array data, confirmed by breakpoint sequencing, showed a maternally inherited deletion that removed the coding exons 14–19 of *IFT74* (Figure 3), a locus encoding a component of the IFT complex that to date has not been associated with BBS or any other ciliopathy. We sequenced all 20 coding exons and splice junctions of *IFT74* in the index case subject and both parents. We identified a paternally inherited heterozygous c.1685−1G>T change (Figure 3). This change maps to the conserved intronic splice acceptor site of exon 20, is absent from 11,868 publicly available healthy control chromosomes (NHLBI Exome Variant Server [EVS]), and was found only once in ~120,000 chromosomes in ExAC. Expanded resequencing of *IFT74* in our 92 BBS-affected individuals yielded only a single additional heterozygous missense change with a minor allele frequency <1% (c.1735G>A [p.Val579Met]; present in 682/120,714 alleles in ExAC) in AR634-03 (Tables 2 and S2).

Data from *Chlamydomonas* and ciliated mammalian cells have shown that IFT74 and IFT81 (MIM: 605489) form a tetrameric complex required for the transport of tubulin within the cilium.[76,77] Ablation of IFT proteins and the concomitant loss of cilia are largely incompatible with life,[78] an expectation inconsistent with our discovery of deleterious mutations in BBS. To understand this apparent paradox, we investigated the pathogenicity of the putative protein product resulting from the 6-exon deletion in AR672. Database analyses showed that the *IFT74* locus encodes two splice isoforms in both human and mouse that utilize different 3′ exons. Notably, the affected individual in AR672 is predicted to have ablated function only for the long isoform, by virtue of the position of both the CNV and the splice site mutation (Figure 3).

To test functionally, the protein resulting from the maternally inherited *IFT74* deletion, we used in vivo complementation in zebrafish embryos.[79] Reciprocal

**Table 3. Breakpoint Features of 18 CNVs Detected in 17 BBS-Affected Case Subjects**

| Sample ID | Gene | hg19 CNV Coordinates | Array Result | Size (bp) | Rearrangement Type | Breakpoint Feature | % Identical Nucleotides | Mechanism |
|---|---|---|---|---|---|---|---|---|
| AR888-03 | *BBS1* | chr11: 66,274,840–66,292,574 | het del: exon1_11 | 17,734 | simple non-recurrent | *AluY - AluY* | 92% | Alu-Alu |
| AR380-03 | *BBS1* | chr11: 66,288,383–66,293,649 | het del: exon9_12 | 5,266 | simple non-recurrent | 1 bp microhomology (T) | no homology | NHEJ/ RBM |
| AR240-03 | *BBS1* | chr11: 66,290,130–66,305,022[a] | het del: exon10_17 | 14,892[a] | NA | - | - | - |
| AR246-03 | *BBS1* | chr11: 66,296,361–66,304,267 | het del: exon14_17 | 7,906 | simple non-recurrent | *AluSp - AluSp* | 87% | Alu-Alu |
| KK047-05 | *BBS2* | chr16: 56,529,926–56,538,197 | hom del: exon8_15[b] | 8,271 | simple non-recurrent | no homology | no homology | NHEJ |
| DM034-004 | *ARL6/BBS3* | chr3: 97,498,355–97,583,359 | hom del: exon4_9[b] | 85,004 | simple non-recurrent | 5 bp microhomology | no homology | NHEJ/ RBM |
| KK11-04 | *ARL6/BBS3* | chr3: 97,508,904–97,513,012 | hom del: exon8[b] | 4,108 | simple non-recurrent | (TG)n simple repeat 41 bp homology | 100% | RBM/SSA |
| 32/3 | *BBS4* | chr15: 73,000,565–73,006,826 | hom del: exon3_4[b] | 6,261 | simple non-recurrent | *AluSc8 - AluSx* | 83% | Alu-Alu |
| AR800-03 | *BBS4* | chr15: 73,006,570–73,014,289 | hom del: exon5_6[b] | 7,719 | simple non-recurrent | 1 bp microhomology | no homology | NHEJ/ RBM |
| AR400-03 | *BBS4* | chr15: 73,006,584–73,012,788 | hom del: exon5_6[b] | 6,204 | simple non-recurrent | *AluSx - AluSg* | 82% | Alu-Alu |
| AR400-03 | *ALMS1* | chr2: 73,617,393–73,789,869 | het del: exon2_15 | 172,476 | simple non-recurrent | 5 bp insertion | no homology | NHEJ/ RBM |
| AR883-04 | *BBS5* | chr2: 170,355,189–170,364,951 | het del: exon8_12 | 9,762 | simple non-recurrent | *AluYc3 - AluSg* | 82% | Alu-Alu |
| AR634-03 | *BBS7* | chr4: 122,749,644–122,750,374 | het del: exon16_17 | 730 | simple non-recurrent | 5 bp insertion | no homology | NHEJ/RBM |
| RC2-03 | *NPHP1* | chr2: 110,875,689–110,967,529[a] | hom del: whole gene[b] | 91,840[a] | recurrent | NA | NA | NAHR |
| 44/3 | *NPHP1* | chr2: 110,875,689–110,967,529[a] | het del: whole gene | 91,840[a] | recurrent | NA | NA | NAHR |
| AR704-03 | *NPHP1* | chr2: 110,875,689–110,967,529[a] | het del: whole gene | 91,840[a] | recurrent | NA | NA | NAHR |
| AR811-03 | *NPHP4* | chr1: 5,910,699–6,038,368[a] | het dup: exon1_28 | 120,535[a] | NA | NA | NA | NA |
| AR811-03 | *NPHP4* | | normal: exon29 | | NA | NA | NA | NA |
| AR811-03 | *NPHP4* | chr1: 6,051,187–6,158,763[a] | het dup: exon30 | 79,389[a] | NA | NA | NA | NA |
| AR672-04 | *IFT74* | chr9: 27,040,563–27,060,990 | het del: exon14_19 | 20,427 | simple non-recurrent | *AluSz - AluY* | 77% | Alu-Alu |

Abbreviations are as follows: NHEJ, non-homologous end joining; RBM, replication-based mechanism; NA, not available; NAHR, nonallelic homologous recombination.
[a]Size and coordinates estimated from the array analysis only.
[b]Homozygous CNVs.

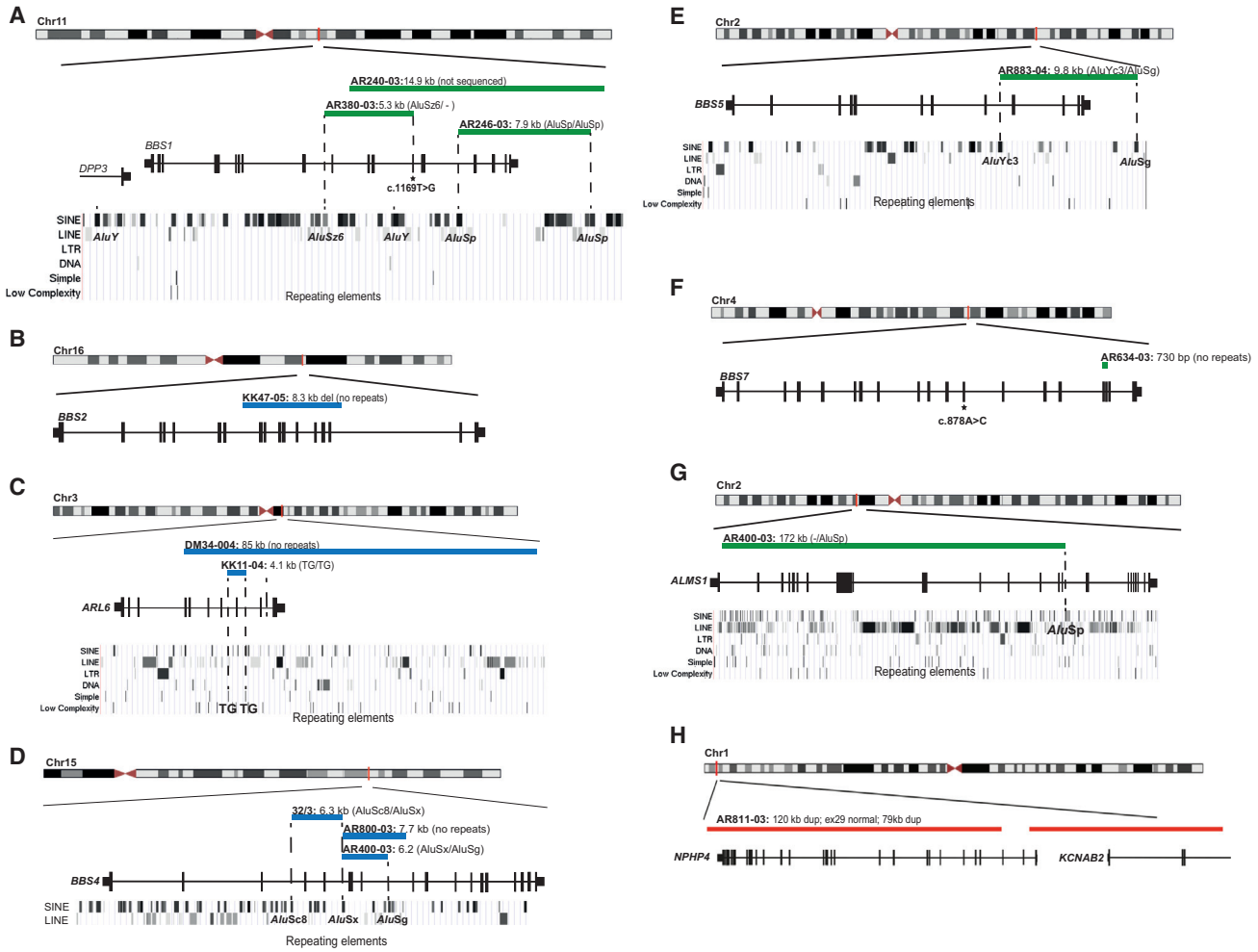


**Figure 1. Schematic of Non-recurrent Exon-Disruptive CNVs Identified in BBS-Affected Case Subjects**
(A) Three heterozygous *BBS1* deletions were identified in *trans* with deleterious point mutations.
(B–D) A single homozygous *BBS2* deletion (B); two homozygous *ARL6/BBS3* deletions (C); and three homozygous *BBS4* deletions (D) were identified in BBS-affected case subjects.
(E) A heterozygous deletion was detected in *BBS5*; no other deleterious variant was detected in *trans*, suggesting that it is a second-site contributor in this individual.
(F) A heterozygous single-exon deletion in *BBS7* was identified in *trans* with a pathogenic SNV.
(G) A heterozygous *ALMS1* deletion was detected in a BBS pedigree harboring a homozygous *BBS4* exon 5–6 deletion (see D).
(H) Identification of a complex duplication encompassing the *NPHP4* locus.
Chromosomal locations are indicated in red (top of each panel); genes, horizontal black lines; exons, vertical black bars (if different transcript isoforms exist, all putative exons are shown); CNVs, horizontal bars (blue, homozygous deletion; green, heterozygous deletion; red, duplication); SNVs, black stars. Repeat elements are shown for *Alu*-mediated CNVs in the relevant panels.

BLAST identified a single zebrafish IFT74 ortholog (51% identity; 71% similarity to human), encoding one annotated transcript against which we designed two different splice-blocking MOs targeting either the splice donor site of *ift74* exon 6 (sb1) or the splice acceptor site of *ift74* exon 4 (sb2), that we used to inject 1- to 4-cell-stage WT embryos (Figure S2; Tables S3 and S4). Suppression of endogenous message conferred by either MO resulted in significant gastrulation defects (shortened body axes, broader and thinner somites, and broad and kinked notochords) in embryo batches scored at the mid-somitic stage ($n = 50–86$ embryos/injection, masked scoring, repeated at least twice, $p < 0.0001$ versus uninjected control), consistent with that reported for other BBS and IFT gene morphants.[9,35,54,80] The phenotype was specific for each of sb1 and sb2, since both could be rescued with the long WT human *IFT74* mRNA isoform ($p < 0.0001$; Figure 4; Table S4) as well as the long isoform harboring a common missense change (c.165A>G [p.Ile55Met]; rs10812505; Table S4). In contrast, the short *IFT74* isoform rescued either of the two *ift74* MOs only partially (Figure 4; Table S4), consistent with the contention that the AR672 proband is hypomorphic for IFT74 function.

Cognizant that some MOs can cause non-specific phenotypes, particularly during gastrulation, we used CRISPR/CAS9 genome editing to target the *ift74* locus in zebrafish. We injected CAS9 protein and guide RNA targeting *ift74* exon 3 into 1-cell-stage embryos and harvested

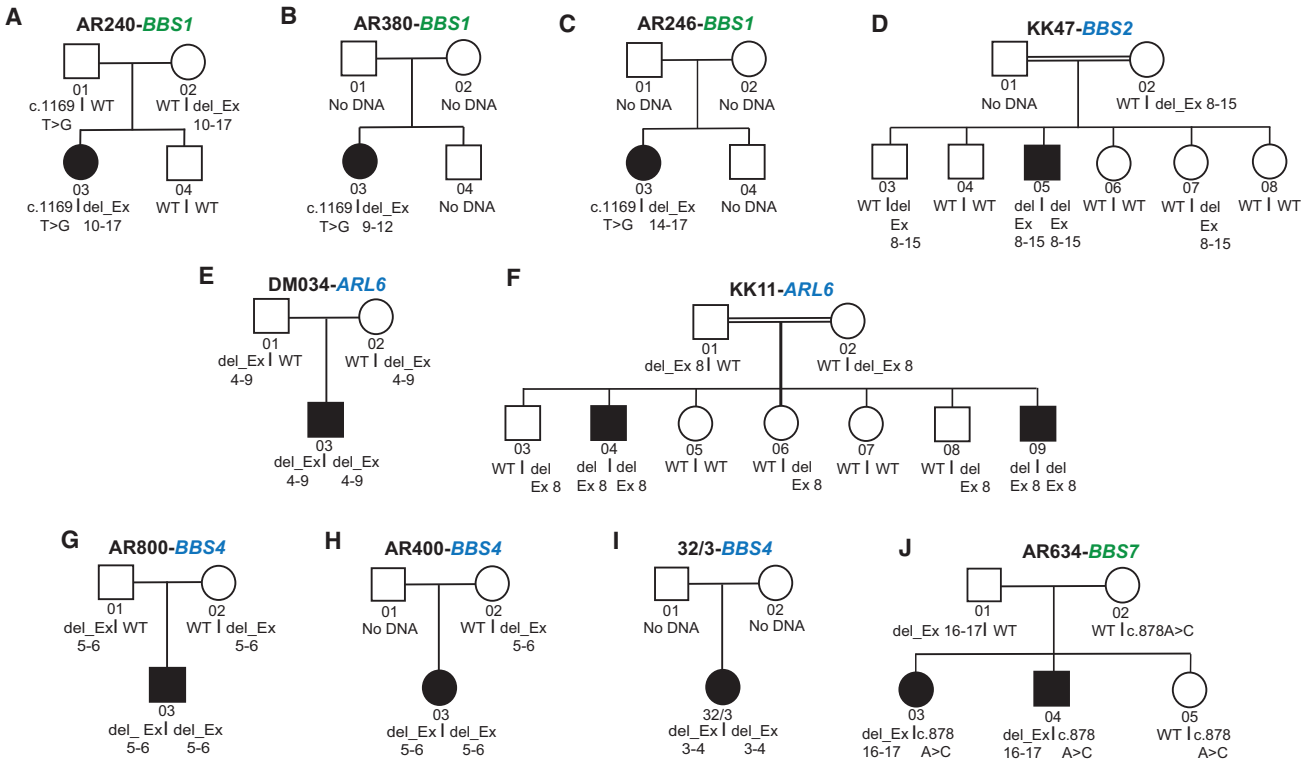


**Figure 2. Pedigrees and Segregation Data of Primary Causal BBS Gene CNVs in Our Cohort**
Segregation analysis results indicate that CNVs can either be sufficient to cause disease (D–I; blue coloring) or Mendelize heterozygous deleterious alleles (A–C, J; green coloring). Squares, males; circles, females; black symbols, individuals affected with BBS; double lines, consanguinity.

embryos at 2 dpf to determine: (1) a high percentage of embryos that expressed mRNA harboring targeting events in *ift74* (8/8 F0 mutants with detectable heteroduplexes in PCR products amplified from the guide RNA target); and (2) an average mosaicism estimated at 43% (11%–75% mosaicism determined from 8–15 clones/embryo; n = 8 F0 mutants; Figure S3). The degree of mosaicism is a likely underestimate, since small deletions will often lead to unstable mRNA transcripts that are eliminated by nonsense-mediated decay. Injection of *ift74* guide RNA and CAS9 protein produced gastrulation defects in midsomitic embryos, phenocopying both *ift74* morphant models; injection of the same dose of guide RNA alone yielded no appreciable phenotypes (n = 39–50 embryos/injection batch, repeated twice; Figure 4).

Next, we sought to investigate the effects of *ift74* depletion on a specific organ system relevant to the BBS clinical spectrum. For this purpose, we evaluated morphants and mutants at 4 dpf for renal abnormalities. Recent reports have shown that IFT complex B zebrafish models, including *ift46* and *ift54* mutants, display dilated pronephric tubules.[81,82] To determine whether this defect was present in *ift74* morphants and mutants, we demarcated renal tubule structures by immunostaining with an anti-$Na^+/K^+$-ATPase antibody, imaged lateral views of larvae, and measured the diameter of a defined tubule region posterior to the proximal convolution (n = 23–54 larvae/batch, repeated; Figure 4). For each of the three *ift74* models (sb1, sb2, and gRNA/CAS9), we observed a significant increase in tubule diameter in comparison to controls ($p < 0.0001$), possibly a consequence of altered fluid flow in the kidney as reported for other *ift* zebrafish models.[83]

## Extensive Oligogenic Load among Individuals Harboring BBS CNVs

Oligogenic inheritance is a hallmark feature of BBS.[24] However, exploration of even that mechanism has been based almost exclusively on sequencing data. Given our current observations on the CNV burden in BBS, and the fact that all affected individuals screened were not preselected for or against prior known pathogenic BBS alleles, we asked how exon-disruptive CNVs and pathogenic SNVs might coalesce in our cohort. First, we expanded our mutational screening efforts to the entire coding exons and splice junctions of *BBS1-16*, *IFT27/BBS19*, and *NPHP1/BBS20* in all 17 individuals harboring CNVs. We confirmed variants in *BBS2*, *MKKS/BBS6*, *BBS7*, *BBS10*, and *NPHP1/BBS20* that were identified in previous candidate gene[11,20] or targeted resequencing[73] studies. Further, we detected ten additional rare alleles that were predicted to disrupt amino acid sequence and were present at <1% minor allele frequency in publicly available databases (13,006 chromosomes; EVS; Tables 2 and S2). With the exceptions of a homozygous 2 bp deletion in *BBS10* (c.2119_2120delGT [p.Val707*])

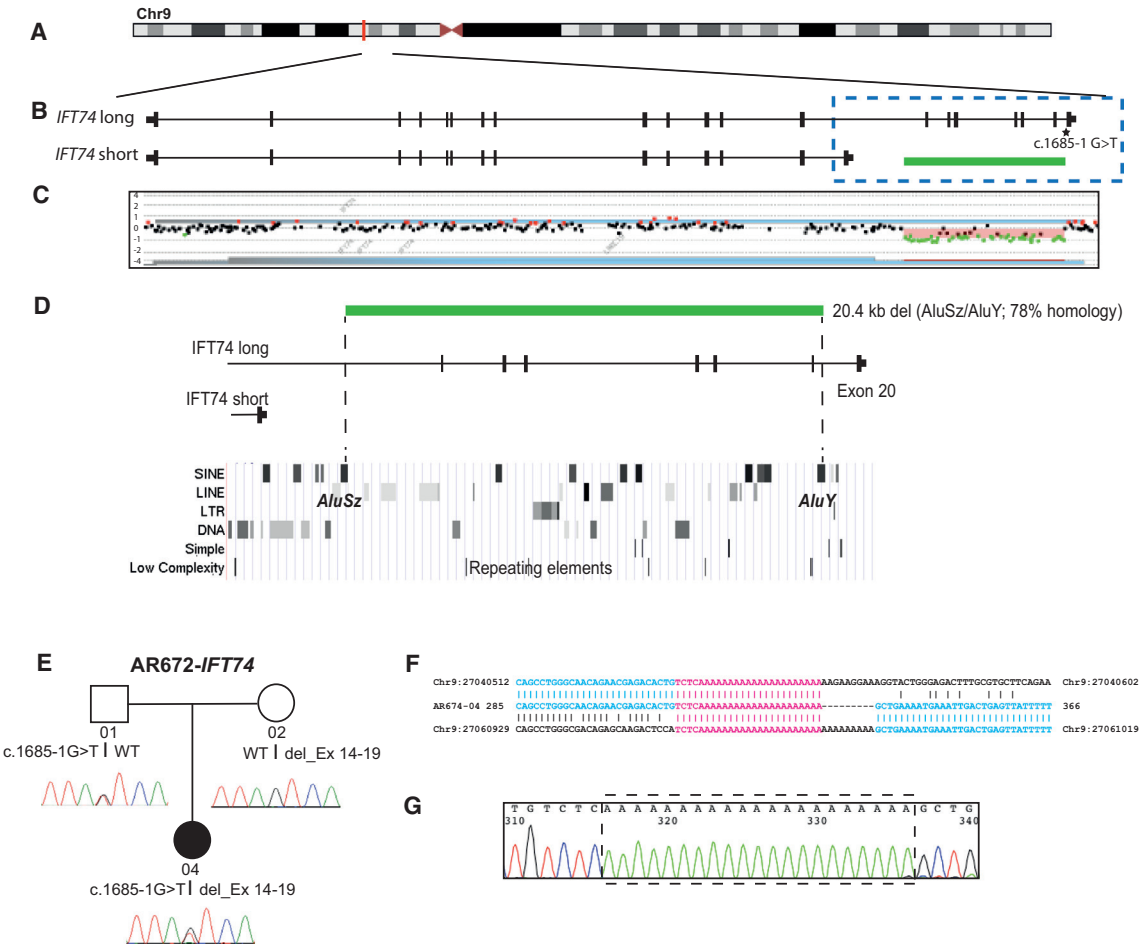


**Figure 3.** ***IFT74*** **Is a Candidate BBS Locus**
(A) Chromosomal location of human *IFT74* on chromosome 9p21 is indicated with a vertical red bar.
(B) Schematic of two *IFT74* transcript variants (long, GenBank: NM_025103.2; short, NM_001099224.1) with alternate 3′ exon usage. Horizontal line, gene locus; vertical black bars, exons; black star, paternally inherited point mutation; green bar, heterozygous deletion.
(C) aCGH plot indicates a heterozygous deletion of ~20 kb encompassing exons 14–19 of the long transcript.
(D) Enlarged view of the CNV- and SNV-bearing region of *IFT74* (corresponds to the dashed blue box in B) and location of *AluSz* and *AluY* repeat elements.
(E) BBS pedigree AR672 and segregation of the paternally inherited c.1685−1G>T splice variant and maternally inherited exon 14–19 deletion.
(F) Breakpoint characterization of the *IFT74* deletion. The junction sequence and corresponding reference location is highlighted in blue and microhomology is shown in red.
(G) Chromatogram corresponding to the microhomology region shown in (F).

that segregated with disease in BBS pedigree AR883 and two heterozygous variants shown previously to be functional null alleles (*BBS5* c.551A>G [p.Asn184Ser] in AR240 and *BBS4* c.137A>G [p.Lys46Arg] in AR634),[54] all other variants were heterozygous missense changes of unknown pathogenic potential. We therefore employed in vivo complementation in zebrafish embryos by established, highly sensitive, and specific assays for *BBS4*, *BBS5*, *BBS7*, *TTC8/BBS8*, *BBS9*, *CEP290/BBS14*, and *SDCCAG8/BBS16*.[9,17,54] Upon masked scoring of embryos rescued with either WT or mutant mRNA (in triplicate), we found that 7 of 7 were pathogenic (Tables 2, S2, S3, S4).

Next, we asked (1) whether CNVs contribute oligogenic alleles to BBS and (2) the extent to which pathogenic BBS gene variation (CNV or SNV) is present in addition to primary recessive loci. Supported by both genetic and in vivo functional data, we have shown previously that the common *NPHP1* deletion can contribute oligogenic alleles to BBS.[11] We found additional such examples (Figures 5 and S4). For instance, in AR883, the proband harbors both a homozygous *BBS10* c.2119_2120delGT mutation (the recessive driver) and a heterozygous *BBS5* exon 8–12 deletion (Figure 5). In other families, we found a range of combinations of deleterious SNVs and CNVs across two or more BBS loci. Overall, of the 17 BBS-affected individuals bearing CNVs, 11 had additional pathogenic mutations in one or more BBS genes in addition to their driver locus. Some of these second sites were SNVs and some were CNVs, with one family harboring as many as four BBS-associated pathogenic alleles (Figures 5, 6, and S4). The

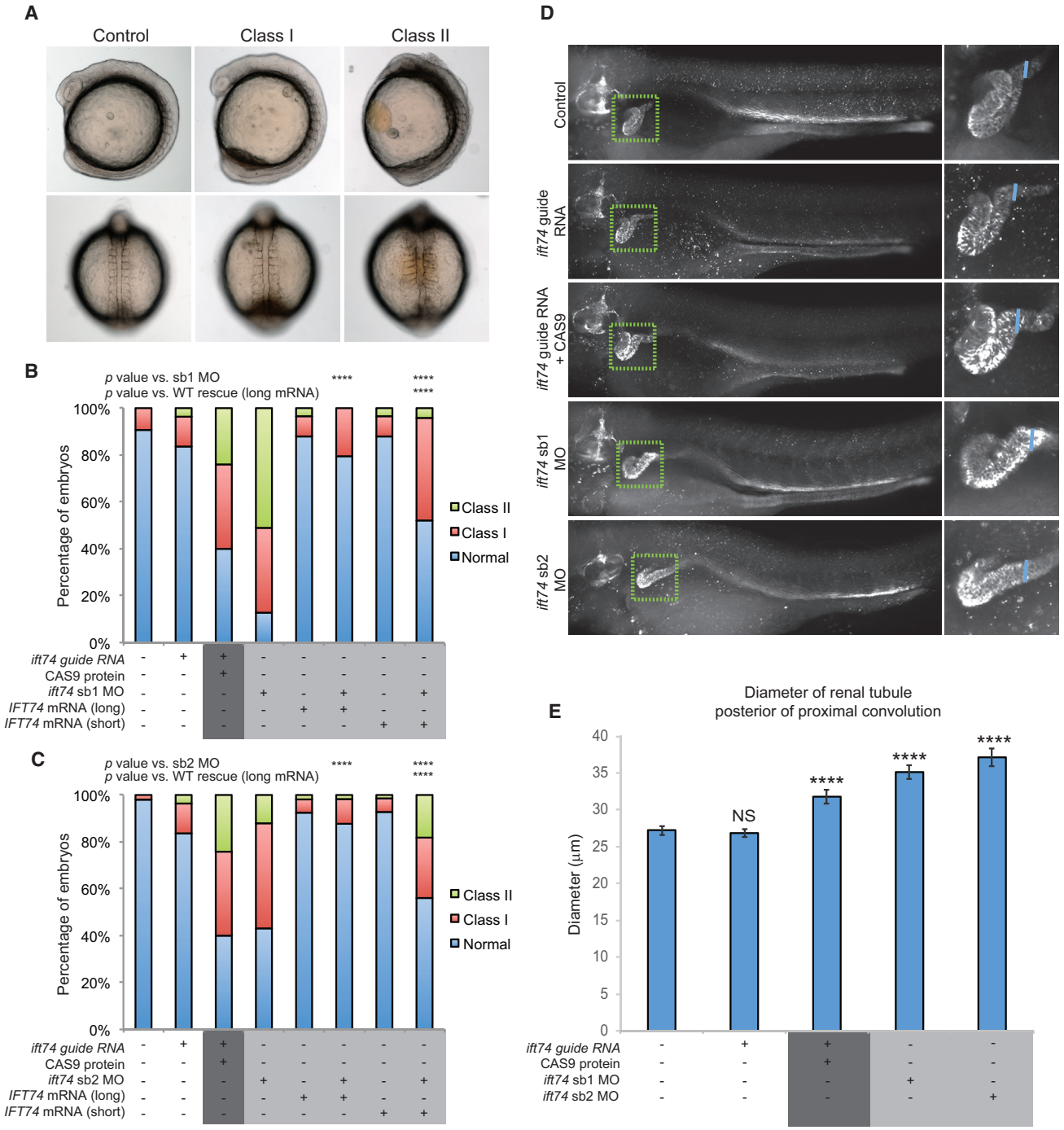


**Figure 4. In Vivo Knockdown or Genome Editing of *ift74* Results in Gastrulation Defects and Renal Phenotypes in Zebrafish**

(A) Representative live images of *ift74* morphant zebrafish embryos at the mid-somitic stage (top, lateral; bottom, dorsal) display gastrulation defects typical of IFT and other ciliary gene suppression models.

(B and C) In vivo complementation studies indicate that the short *IFT74* transcript is a hypomorphic allele; n = 39–86 embryos/injection batch; masked scoring, repeated at least twice; statistical significance was determined using a $\chi^2$ test to compare injected batches versus controls; *p < 0.0001; NS, not significant; WT, wild-type.

(D) Fixed 4 day post fertilization larvae were immunostained with anti-$Na^+/K^+$ ATPase antibody to mark renal tubules, representative images are shown for each of the *ift74* morphant and mutant models; green dashed boxes indicate region of inset; blue lines indicates the location of the renal tubule diameter measured on lateral images.

(E) Quantification of renal phenotypes in larvae injected with 50 pg guide RNA alone; 50 pg guide RNA/200 pg CAS9 protein; 9 ng *ift74* sb1 or 9 ng *ift74* sb2 MO demonstrate an increased diameter of the proximal convoluted tubule in comparison to controls; n = 23–54 per condition, repeated; statistical significance was determined by a Student's t test to compare injected batches versus controls. NS, not significant; ****p < 0.0001. Error bars represent standard error of the mean (SEM).

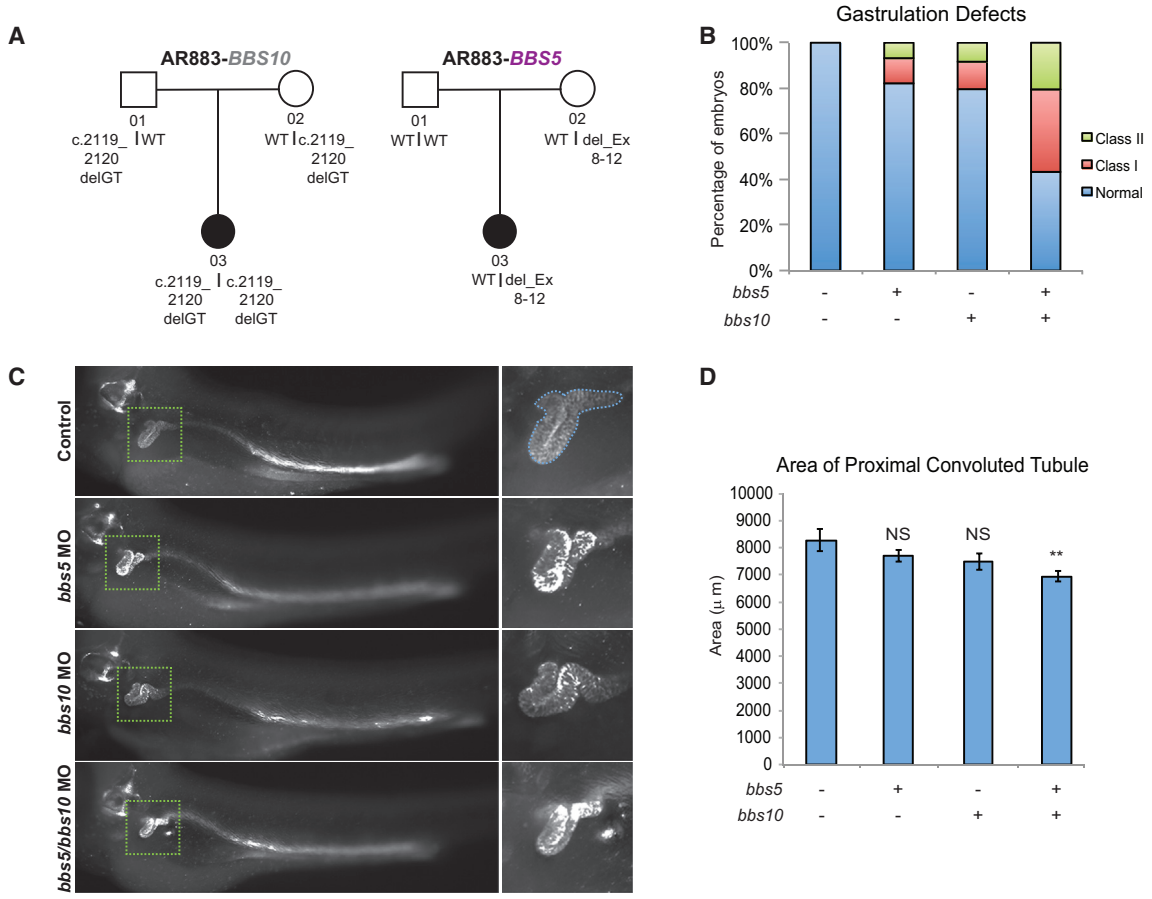


**Figure 5. Segregation and In Vivo Analysis of Oligogenic BBS Loci Demonstrate Epistatic Effects**

AR883-03 harbors a heterozygous *BBS5* CNV that is a likely second-site contributor to disease caused by mutation at the primary causal locus *BBS10*.

(A) Pedigree and segregation of each BBS gene variant (CNV or SNV; separate pedigrees for each gene) with the primary locus harboring causal variants shown on the far left. Gene name color indicates heterozygous deletion CNV (magenta) or point mutation (gray).

(B) Bar chart indicates in vivo assessment of *bbs* gene interaction by the comparison of either single-gene or pairwise injection of sub-effective doses of MOs and phenotypic scoring of zebrafish embryo batches at the mid-somitic stage. Objective scoring criteria correspond to images shown in Figure 4A and demonstrate an epistatic effect in the double-MO batch. See Table S5 for embryo counts and additional examples.

(C) A second phenotypic readout, area of proximal convoluted tubule measured at 4 days post fertilization, demonstrates epistatic effects of *bbs* gene interaction. Fixed larvae were immunostained with anti-$Na^+/K^+$ ATPase antibody; green dashed box indicates region of inset; blue dashed line indicates the region of the proximal convoluted tubule measured on lateral images.

(D) Quantification of renal phenotypes in single or double MO-injected larvae demonstrate a progressive reduction in the size of the proximal convoluted tubule; n = 34–46 per condition, repeated; statistical significance was determined by a Student's t test to compare injected batches versus controls. NS, not significant; **$p < 0.01$. Error bars represent standard error of the mean (SEM).

enrichment of oligogenic CNVs in the BBS cohort remained significant after removing CNVs considered to be primary causal alleles under a recessive paradigm (Table 2). We observed a total of five heterozygous oligogenic CNVs in affected individuals (AR883-04/*BBS5*; AR811-03/*NPHP4*; AR400-03/*ALMS1*; and the previously reported *NPHP1* deletion in 44/3 and AR704-03;[11] Table 2; Figure 6) and one heterozygous deletion in control subjects (5/184 for BBS chromosomes versus 1/458 for control chromosomes; $p = 0.0085$, Fisher's exact test).

### In Vivo Analysis of Oligogenic BBS Loci

Genetic interaction has been assessed extensively among the BBS-associated genes and in concert with other ciliopathy loci.[9,11,20,21,35,54,84,85] To investigate whether the pairwise BBS-associated gene combinations seen here result in additive or epistatic effects, we co-injected sub-effective doses of MO targeting the orthologous zebrafish genes, and we compared the fraction of affected embryos scored at the mid-somitic stage to that of embryos injected with single-gene MO concentrations alone. To approximate the BBS mutational burden in affected individuals, we tested four pairwise gene suppression combinations; we also generated an additional model in which we suppressed three BBS-associated genes simultaneously (Figures 5 and S4; Tables 2 and S5). In three instances, and consistent with our previous observations of *nphp1* interactions with *bbs1*, *bbs2*, *bbs7*, and *bbs10*,[11] we observed an additive

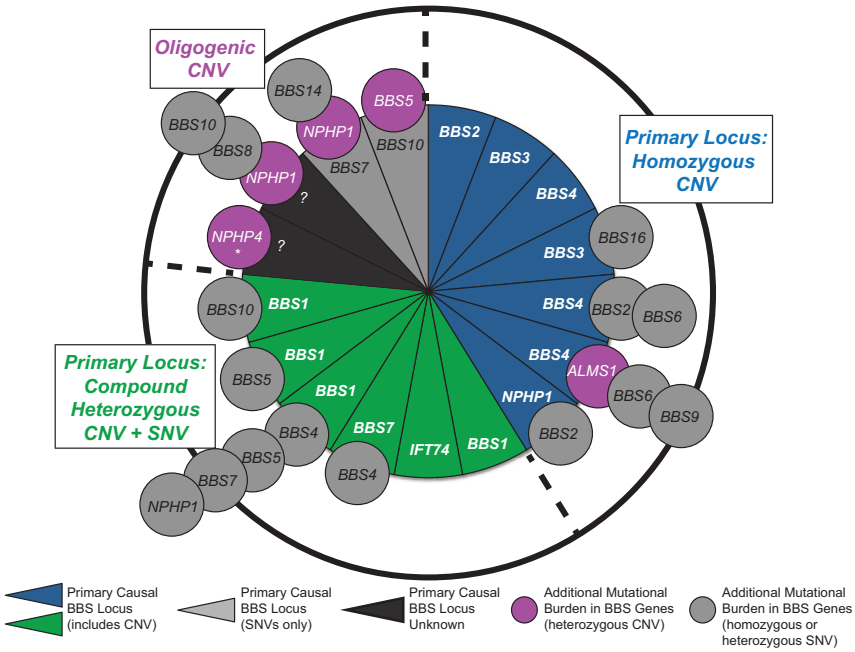


**Figure 6. Genetic Architecture of BBS Gene Variation in 17 BBS-Affected Case Subjects Harboring CNVs**

Each slice of the pie chart represents one BBS-affected case subject and the primary BBS locus harboring causal variants is indicated with gene names and colors (homozygous CNV, blue; compound heterozygous CNV + SNV, green; homozygous or compound heterozygous SNV, gray). Circles overlapping each slice represent the additional mutational burden in each BBS-affected case subject (CNV, magenta; SNV, gray). 5/17 individuals (29%) harbor no additional BBS gene variants outside their primary causal driver; 12/17 individuals (71%) have 1–4 additional heterozygous deleterious variants in *BBS1-16*, *IFT27/BBS19*, or *NPHP1*. Asterisk (*) indicates duplication CNV.

effect. However, in one pairwise (*bbs5* and *bbs10*) and one triple (*bbs2*, *bbs4*, and *bbs6*) gene suppression model, we saw an epistatic effect in which the combined gene suppression model exhibits increased percentages of phenotypic severity, especially class II (severe) in comparison to the addition of any of the single suppression models alone (Figures 5 and S4). We corroborated these epistatic interactions in 4 dpf zebrafish larvae, building on our previous study of *bbs* gene interaction with a BBS candidate locus, *nphp1*.[11] In contrast to *ift* models, which display dilated pronephric tubules, we have shown previously that suppression of *bbs* results in atrophy and diminished convolution of the proximal tubule.[11] Immunostaining of renal structures and measurement of lateral images of the proximal convoluted tubule from the *bbs5/bbs10* or *bbs2/bbs4/bbs6* genetic interaction models showed a reduction in the size of the proximal convoluted tubule in the combined model in comparison to any of the single MO-injected batches alone (Figures 5 and S4). These exacerbated phenotypic effects are not likely to be underscored by altered *bbs* expression in the presence of excess MO dosing; qPCR studies from representative single, double, or triple MO injected batches showed no significant differences in *bbs* expression in comparison to controls (Figure S5).

Finally, we used this approach to test the oligogenic contribution of the heterozygous *ALMS1* CNV detected in BBS pedigree AR400. The proband harbors a recessive *BBS4* locus (homozygous exon 5–6 deletion) in addition to a heterozygous *BBS9* c.1993C>T (p.Leu665Phe) probably functional null allele and a heterozygous *ALMS1* exon 2–15 deletion. To model the combined effects of these loci, we first developed a zebrafish model of *alms1* suppression (Figure S2). We targeted the sole ALMS1 ortholog in zebrafish with an sb-MO and coinjected subeffective doses into embryo batches either alone or in combination with *bbs4* and/or *bbs9* MOs. In midsomite-stage embryos, we found an additive effect, suggesting that ALMS1 is neither redundant with the other two BBS-associated proteins nor does it exacerbate significantly the phenotypic severity (Table S5). Together, these data substantiate further the complexity of the genetic architecture of BBS and lend further support to the contribution of mutational burden, in addition to primary recessive loci.

## Discussion

Genetic and functional studies of the ciliopathies have informed the complexity of biological systems with regard to phenotypic variability and have afforded us the opportunity to begin to understand how the distribution of mutations beyond the primary causal locus can influence penetrance and expressivity.[23] However, essentially all that work was driven by mutational data derived by sequencing; some examples notwithstanding, the contribution of CNVs to both causality and overall mutational burden has been under-recognized. Here, using a high-density aCGH with sub-kb resolution to test an unselected cohort of BBS individuals, we have found that 18% of these individuals harbor at least one exon-disruptive CNV. These lesions, which range in size from ~700 bp to >100 kb, can contribute recessive alleles; can Mendelize pathogenic SNVs on the other chromosome; and probably can interact with both CNVs and SNVs in other BBS loci, a posit substantiated by genetic interaction of the discovered BBS-associated gene combinations in vivo. Of note, analyses of either control databases or intramural studies of control samples on the same platform as our discovery cohort showed a stark absence of such CNVs from the general population, indicating that this CNV enrichment is unlikely to represent random background variation. Even

so, the study of larger cohorts, both for BBS and other ciliopathies, will be required to measure the precise contribution of CNVs to both recessive and oligogenic paradigms.

We also note that the observed genetic interactions did not always lead to the same magnitude of effect, as measured by the severity of the combinatorial suppression of two or more *bbs* genes in zebrafish embryos evaluated at two different stages of development. Acknowledging that the interaction experiments in zebrafish embryos are a coarse approximation of the genetic architecture of these specific BBS allelic contributions to trait manifestation in case subjects, we speculate that these patterns, once understood more fully, have the potential to inform the effect of *trans* alleles on phenotypic expression (an exercise that the current cohort is underpowered to accomplish). Moreover, we recognize that not all genetic interactions will necessarily be deleterious. In that context, the analysis of individuals with clinically mild ciliopathies, or individuals protected from a specific organ disorder within the ciliopathy spectrum, might be informative at documenting protective CNV/SNV combinations.

Finally, our studies highlight the continued utility of CNV analysis to identify driver loci. In addition to previous studies that identified recessive CNVs in *NPHP1* in BBS and *ARMC4* (MIM: 615408) in primary ciliary dyskinesia (PCD [MIM: 615451][11,86]), examination of the non-deleted chromosome identified *IFT74* as a likely BBS locus. We discovered a single nuclear family; sequencing of the remainder of our cohort identified a sole rare SNV at this locus, functional testing of which showed it to be benign (Table S4). Therefore, we remain cautious until additional affected individuals are identified. Nonetheless, several lines of evidence support the candidacy of this locus. First, this is not the first IFT component to be mutated in this disorder; mutations in *IFT27* and *IFT172* were shown recently in BBS sibships.[1,22] Second, not only are the mutations likely damaging and potentially clinically severe for their functional impact (deletion/splice), but both mutant alleles affect specifically the long isoform of this gene, rendering the index case a functional hypomorph for this locus, offering an attractive hypothesis to explain the milder phenotype in this family compared to the severe, often prenatal or perinatal, lethal phenotypes caused by recessive null alleles in IFT genes in humans or model organisms.[78,80,87,88] Thus, it will be important to determine the differential functions of the two IFT74 splice isoforms, including their spatiotemporal distribution (and relative ratios across different tissues); as well as their interacting partners and cargo, since these might inform pathomechanism. Of note, the renal pathology of our zebrafish *ift74* model might predict a dilatation defect in humans, which is different from the dysplastic phenotypes seen in other BBS models; clinical assessment of additional BBS-affected families with IFT mutations will be required to test this hypothesis.

In conclusion, our studies have highlighted a substantial role for CNVs in BBS. In addition to improving our appreciation of the complexity of the genetic architecture of this and other ciliopathies, our observations also highlight two critical points for clinical molecular diagnosis. First, our data highlight the need to consider all types of genetic and genomic lesions that can impact gene and protein function. Computational algorithms that rely on depth of coverage[89,90] could not have detected most of the deletions that we discovered due to their small size, and the same is true for some of the commonly used techniques in molecular cytogenetic laboratories.[91] It is possible that the eventual transition to whole-genome diagnostic sequencing will improve the accuracy of detection of such structural variants. Second, our data also emphasize why it remains important to continue the study of the exomes and genomes of affected individuals beyond the discovery of a primary disease driver. Even though most current human genetic studies lack the resolution to interpret the effect of alleles beyond the recessive locus, the accrual of bona fide deleterious lesions in biological systems will ultimately inform the management of individuals who have the same recessive alleles but divergent clinical presentations.

## Supplemental Data

Supplemental Data include five figures and five tables and can be found with this article online at http://dx.doi.org/10.1016/j.ajhg.2015.04.023.

## Acknowledgments

We thank the individuals with BBS and their families for their continued participation in our studies. We also thank Richard Gibbs and Donna Muzny for assistance with sequence analysis and advice, Christelle Golzio for assistance in designing and developing CRISPR protocols, and Julien Philippe for assistance with the analysis of qPCR data. This work was funded by NIH grants DK075972, HD042601, and DK096415 (N.K.), DK072301 and DK096493 (N.K. and E.E.D.), EY021872 (E.E.D.), and NS058529 and HG006542 (J.R.L.); the Conselho Nacional de Desenvolvimento Científico e Tecnológico (CNPq) through the Young Investigator fellowship (Science without Borders Program) grant 402520/2012-2 to C.M.B.C.; funding from EU 7th FP under GA nr. 241955, project SYSCILIA to N.K.; and by the Swedish Research Council grants 2010-978 and 2012-1526 (A.L.). R.A.L. is a Senior Scientific Investigator of Research to Prevent Blindness, whose unrestricted funds supported parts of these investigations. N.K. is a distinguished Jean and George Brumley Professor. J.R.L. has stock ownership in 23andMe, is a paid consultant for Regeneron Pharmaceuticals, has stock options in Lasergen, Inc., is a co-inventor on multiple United States and European patents related to molecular diagnostics for inherited neuropathies, eye diseases, and bacterial genomic fingerprinting, and is on the Scientific Advisory Board of Baylor Genetics. N.K. is a paid consultant for and holds significant stock of Rescindo Therapeutics, Inc.

Received: April 1, 2015
Accepted: June 13, 2016
Published: August 4, 2016

## Web Resources

Coriell Cell Repositories, https://catalog.coriell.org/
CRISPR design tool, http://crispr.mit.edu
Database of Genomic Variants (DGV), http://dgv.tcag.ca/dgv/app/home
ExAC Browser, http://exac.broadinstitute.org/
GenBank, http://www.ncbi.nlm.nih.gov/genbank/
MutationTaster, http://www.mutationtaster.org/
NHLBI Exome Sequencing Project (ESP) Exome Variant Server, http://evs.gs.washington.edu/EVS/
OMIM, http://www.omim.org/
PolyPhen-2, http://genetics.bwh.harvard.edu/pph2/
SIFT, http://sift.bii.a-star.edu.sg/

## References


1. Aldahmesh, M.A., Li, Y., Alhashem, A., Anazi, S., Alkuraya, H., Hashem, M., Awaji, A.A., Sogaty, S., Alkharashi, A., Alzahrani, S., et al. (2014). IFT27, encoding a small GTPase component of IFT particles, is mutated in a consanguineous family with Bardet-Biedl syndrome. Hum. Mol. Genet. *23*, 3307–3315.
2. Ansley, S.J., Badano, J.L., Blacque, O.E., Hill, J., Hoskins, B.E., Leitch, C.C., Kim, J.C., Ross, A.J., Eichers, E.R., Teslovich, T.M., et al. (2003). Basal body dysfunction is a likely cause of pleiotropic Bardet-Biedl syndrome. Nature *425*, 628–633.
3. Badano, J.L., Ansley, S.J., Leitch, C.C., Lewis, R.A., Lupski, J.R., and Katsanis, N. (2003). Identification of a novel Bardet-Biedl syndrome protein, BBS7, that shares structural features with BBS1 and BBS2. Am. J. Hum. Genet. *72*, 650–658.
4. Chiang, A.P., Beck, J.S., Yen, H.J., Tayeh, M.K., Scheetz, T.E., Swiderski, R.E., Nishimura, D.Y., Braun, T.A., Kim, K.Y., Huang, J., et al. (2006). Homozygosity mapping with SNP arrays identifies TRIM32, an E3 ubiquitin ligase, as a Bardet-Biedl syndrome gene (BBS11). Proc. Natl. Acad. Sci. USA *103*, 6287–6292.
5. Chiang, A.P., Nishimura, D., Searby, C., Elbedour, K., Carmi, R., Ferguson, A.L., Secrist, J., Braun, T., Casavant, T., Stone, E.M., and Sheffield, V.C. (2004). Comparative genomic analysis identifies an ADP-ribosylation factor-like gene as the cause of Bardet-Biedl syndrome (BBS3). Am. J. Hum. Genet. *75*, 475–484.
6. Fan, Y., Esmail, M.A., Ansley, S.J., Blacque, O.E., Boroevich, K., Ross, A.J., Moore, S.J., Badano, J.L., May-Simera, H., Compton, D.S., et al. (2004). Mutations in a member of the Ras superfamily of small GTP-binding proteins causes Bardet-Biedl syndrome. Nat. Genet. *36*, 989–993.
7. Katsanis, N., Beales, P.L., Woods, M.O., Lewis, R.A., Green, J.S., Parfrey, P.S., Ansley, S.J., Davidson, W.S., and Lupski, J.R. (2000). Mutations in MKKS cause obesity, retinal dystrophy and renal malformations associated with Bardet-Biedl syndrome. Nat. Genet. *26*, 67–70.
8. Kim, S.K., Shindo, A., Park, T.J., Oh, E.C., Ghosh, S., Gray, R.S., Lewis, R.A., Johnson, C.A., Attie-Bittach, T., Katsanis, N., and Wallingford, J.B. (2010). Planar cell polarity acts through septins to control collective cell movement and ciliogenesis. Science *329*, 1337–1340.
9. Leitch, C.C., Zaghloul, N.A., Davis, E.E., Stoetzel, C., Diaz-Font, A., Rix, S., Alfadhel, M., Lewis, R.A., Eyaid, W., Banin, E., et al. (2008). Hypomorphic mutations in syndromic encephalocele genes are associated with Bardet-Biedl syndrome. Nat. Genet. *40*, 443–448.
10. Li, J.B., Gerdes, J.M., Haycraft, C.J., Fan, Y., Teslovich, T.M., May-Simera, H., Li, H., Blacque, O.E., Li, L., Leitch, C.C., et al. (2004). Comparative genomics identifies a flagellar and basal body proteome that includes the BBS5 human disease gene. Cell *117*, 541–552.
11. Lindstrand, A., Davis, E.E., Carvalho, C.M., Pehlivan, D., Willer, J.R., Tsai, I.C., Ramanathan, S., Zuppan, C., Sabo, A., Muzny, D., et al. (2014). Recurrent CNVs and SNVs at the NPHP1 locus contribute pathogenic alleles to Bardet-Biedl syndrome. Am. J. Hum. Genet. *94*, 745–754.
12. Marion, V., Stutzmann, F., Gérard, M., De Melo, C., Schaefer, E., Claussmann, A., Hellé, S., Delague, V., Souied, E., Barrey, C., et al. (2012). Exome sequencing identifies mutations in LZTFL1, a BBSome and smoothened trafficking regulator, in a family with Bardet–Biedl syndrome with situs inversus and insertional polydactyly. J. Med. Genet. *49*, 317–321.
13. Mykytyn, K., Braun, T., Carmi, R., Haider, N.B., Searby, C.C., Shastri, M., Beck, G., Wright, A.F., Iannaccone, A., Elbedour, K., et al. (2001). Identification of the gene that, when mutated, causes the human obesity syndrome BBS4. Nat. Genet. *28*, 188–191.
14. Mykytyn, K., Nishimura, D.Y., Searby, C.C., Shastri, M., Yen, H.J., Beck, J.S., Braun, T., Streb, L.M., Cornier, A.S., Cox, G.F., et al. (2002). Identification of the gene (BBS1) most commonly involved in Bardet-Biedl syndrome, a complex human obesity syndrome. Nat. Genet. *31*, 435–438.
15. Nishimura, D.Y., Searby, C.C., Carmi, R., Elbedour, K., Van Maldergem, L., Fulton, A.B., Lam, B.L., Powell, B.R., Swiderski, R.E., Bugge, K.E., et al. (2001). Positional cloning of a novel gene on chromosome 16q causing Bardet-Biedl syndrome (BBS2). Hum. Mol. Genet. *10*, 865–874.
16. Nishimura, D.Y., Swiderski, R.E., Searby, C.C., Berg, E.M., Ferguson, A.L., Hennekam, R., Merin, S., Weleber, R.G., Biesecker, L.G., Stone, E.M., and Sheffield, V.C. (2005). Comparative genomics and gene expression analysis identifies BBS9, a new Bardet-Biedl syndrome gene. Am. J. Hum. Genet. *77*, 1021–1033.
17. Otto, E.A., Hurd, T.W., Airik, R., Chaki, M., Zhou, W., Stoetzel, C., Patil, S.B., Levy, S., Ghosh, A.K., Murga-Zamalloa, C.A., et al. (2010). Candidate exome capture identifies mutation of SDCCAG8 as the cause of a retinal-renal ciliopathy. Nat. Genet. *42*, 840–850.
18. Scheidecker, S., Etard, C., Pierce, N.W., Geoffroy, V., Schaefer, E., Muller, J., Chennen, K., Flori, E., Pelletier, V., Poch, O., et al. (2014). Exome sequencing of Bardet-Biedl syndrome patient identifies a null mutation in the BBSome subunit BBIP1 (BBS18). J. Med. Genet. *51*, 132–136.
19. Slavotinek, A.M., Stone, E.M., Mykytyn, K., Heckenlively, J.R., Green, J.S., Heon, E., Musarella, M.A., Parfrey, P.S., Sheffield, V.C., and Biesecker, L.G. (2000). Mutations in MKKS cause Bardet-Biedl syndrome. Nat. Genet. *26*, 15–16.
20. Stoetzel, C., Laurier, V., Davis, E.E., Muller, J., Rix, S., Badano, J.L., Leitch, C.C., Salem, N., Chouery, E., Corbani, S., et al. (2006). BBS10 encodes a vertebrate-specific chaperonin-like protein and is a major BBS locus. Nat. Genet. *38*, 521–524.
21. Stoetzel, C., Muller, J., Laurier, V., Davis, E.E., Zaghloul, N.A., Vicaire, S., Jacquelin, C., Plewniak, F., Leitch, C.C., Sarda, P., et al. (2007). Identification of a novel BBS gene (BBS12) highlights the major role of a vertebrate-specific branch of chaperonin-related proteins in Bardet-Biedl syndrome. Am. J. Hum. Genet. *80*, 1–11.
22. Bujakowska, K.M., Zhang, Q., Siemiatkowska, A.M., Liu, Q., Place, E., Falk, M.J., Consugar, M., Lancelot, M.E., Antonio,

A., Lonjou, C., et al. (2015). Mutations in IFT172 cause isolated retinal degeneration and Bardet-Biedl syndrome. Hum. Mol. Genet. *24*, 230–242.
23. Davis, E.E., and Katsanis, N. (2012). The ciliopathies: a transitional model into systems biology of human genetic disease. Curr. Opin. Genet. Dev. *22*, 290–303.
24. Zaghloul, N.A., and Katsanis, N. (2009). Mechanistic insights into Bardet-Biedl syndrome, a model ciliopathy. J. Clin. Invest. *119*, 428–437.
25. den Hollander, A.I., Koenekoop, R.K., Yzer, S., Lopez, I., Arends, M.L., Voesenek, K.E., Zonneveld, M.N., Strom, T.M., Meitinger, T., Brunner, H.G., et al. (2006). Mutations in the CEP290 (NPHP6) gene are a frequent cause of Leber congenital amaurosis. Am. J. Hum. Genet. *79*, 556–561.
26. Karmous-Benailly, H., Martinovic, J., Gubler, M.C., Sirot, Y., Clech, L., Ozilou, C., Auge, J., Brahimi, N., Etchevers, H., Detrait, E., et al. (2005). Antenatal presentation of Bardet-Biedl syndrome may mimic Meckel syndrome. Am. J. Hum. Genet. *76*, 493–504.
27. Sayer, J.A., Otto, E.A., O'Toole, J.F., Nurnberg, G., Kennedy, M.A., Becker, C., Hennies, H.C., Helou, J., Attanasio, M., Fausett, B.V., et al. (2006). The centrosomal protein nephrocystin-6 is mutated in Joubert syndrome and activates transcription factor ATF4. Nat. Genet. *38*, 674–681.
28. Valente, E.M., Silhavy, J.L., Brancati, F., Barrano, G., Krishnaswami, S.R., Castori, M., Lancaster, M.A., Boltshauser, E., Boccone, L., Al-Gazali, L., et al.; International Joubert Syndrome Related Disorders Study Group (2006). Mutations in CEP290, which encodes a centrosomal protein, cause pleiotropic forms of Joubert syndrome. Nat. Genet. *38*, 623–625.
29. Aliferis, K., Hellé, S., Gyapay, G., Duchatelet, S., Stoetzel, C., Mandel, J.L., and Dollfus, H. (2012). Differentiating Alström from Bardet-Biedl syndrome (BBS) using systematic ciliopathy genes sequencing. Ophthalmic Genet. *33*, 18–22.
30. Pereiro, I., Hoskins, B.E., Marshall, J.D., Collin, G.B., Naggert, J.K., Piñeiro-Gallego, T., Oitmaa, E., Katsanis, N., Valverde, D., and Beales, P.L. (2011). Arrayed primer extension technology simplifies mutation detection in Bardet-Biedl and Alström syndrome. Eur. J. Hum. Genet. *19*, 485–488.
31. Katsanis, N. (2004). The oligogenic properties of Bardet-Biedl syndrome. Hum. Mol. Genet. *13*, R65–R71.
32. Katsanis, N., Ansley, S.J., Badano, J.L., Eichers, E.R., Lewis, R.A., Hoskins, B.E., Scambler, P.J., Davidson, W.S., Beales, P.L., and Lupski, J.R. (2001). Triallelic inheritance in Bardet-Biedl syndrome, a Mendelian recessive disorder. Science *293*, 2256–2259.
33. Katsanis, N., Eichers, E.R., Ansley, S.J., Lewis, R.A., Kayserili, H., Hoskins, B.E., Scambler, P.J., Beales, P.L., and Lupski, J.R. (2002). BBS4 is a minor contributor to Bardet-Biedl syndrome and may also participate in triallelic inheritance. Am. J. Hum. Genet. *71*, 22–29.
34. Muller, J., Stoetzel, C., Vincent, M.C., Leitch, C.C., Laurier, V., Danse, J.M., Hellé, S., Marion, V., Bennouna-Greene, V., Vicaire, S., et al. (2010). Identification of 28 novel mutations in the Bardet-Biedl syndrome genes: the burden of private mutations in an extensively heterogeneous disease. Hum. Genet. *127*, 583–593.
35. Davis, E.E., Zhang, Q., Liu, Q., Diplas, B.H., Davey, L.M., Hartley, J., Stoetzel, C., Szymanska, K., Ramaswami, G., Logan, C.V., et al.; NISC Comparative Sequencing Program (2011). TTC21B contributes both causal and modifying alleles across the ciliopathy spectrum. Nat. Genet. *43*, 189–196.
36. Khanna, H., Davis, E.E., Murga-Zamalloa, C.A., Estrada-Cuzcano, A., Lopez, I., den Hollander, A.I., Zonneveld, M.N., Othman, M.I., Waseem, N., Chakarova, C.F., et al. (2009). A common allele in RPGRIP1L is a modifier of retinal degeneration in ciliopathies. Nat. Genet. *41*, 739–745.
37. Louie, C.M., Caridi, G., Lopes, V.S., Brancati, F., Kispert, A., Lancaster, M.A., Schlossman, A.M., Otto, E.A., Leitges, M., Gröne, H.J., et al. (2010). AHI1 is required for photoreceptor outer segment development and is a modifier for retinal degeneration in nephronophthisis. Nat. Genet. *42*, 175–180.
38. Rachel, R.A., May-Simera, H.L., Veleri, S., Gotoh, N., Choi, B.Y., Murga-Zamalloa, C., McIntyre, J.C., Marek, J., Lopez, I., Hackett, A.N., et al. (2012). Combining Cep290 and Mkks ciliopathy alleles in mice rescues sensory defects and restores ciliogenesis. J. Clin. Invest. *122*, 1233–1245.
39. Migliavacca, E., Golzio, C., Männik, K., Blumenthal, I., Oh, E.C., Harewood, L., Kosmicki, J.A., Loviglio, M.N., Giannuzzi, G., Hippolyte, L., et al.; 16p11.2 European Consortium (2015). A potential contributory role for ciliary dysfunction in the 16p11.2 600 kb BP4-BP5 pathology. Am. J. Hum. Genet. *96*, 784–796.
40. Stankiewicz, P., and Lupski, J.R. (2010). Structural variation in the human genome and its role in disease. Annu. Rev. Med. *61*, 437–455.
41. Lupski, J.R. (2009). Genomic disorders ten years on. Genome Med. *1*, 42.
42. Lupski, J.R. (1998). Genomic disorders: structural features of the genome can lead to DNA rearrangements and human disease traits. Trends Genet. *14*, 417–422.
43. Boone, P.M., Bacino, C.A., Shaw, C.A., Eng, P.A., Hixson, P.M., Pursley, A.N., Kang, S.H., Yang, Y., Wiszniewska, J., Nowakowska, B.A., et al. (2010). Detection of clinically relevant exonic copy-number changes by array CGH. Hum. Mutat. *31*, 1326–1342.
44. Zhang, F., Khajavi, M., Connolly, A.M., Towne, C.F., Batish, S.D., and Lupski, J.R. (2009). The DNA replication FoSTeS/MMBIR mechanism can generate genomic, genic and exonic complex rearrangements in humans. Nat. Genet. *41*, 849–853.
45. Boone, P.M., Campbell, I.M., Baggett, B.C., Soens, Z.T., Rao, M.M., Hixson, P.M., Patel, A., Bi, W., Cheung, S.W., Lalani, S.R., et al. (2013). Deletions of recessive disease genes: CNV contribution to carrier states and disease-causing alleles. Genome Res. *23*, 1383–1394.
46. Chen, J., Smaoui, N., Hammer, M.B., Jiao, X., Riazuddin, S.A., Harper, S., Katsanis, N., Riazuddin, S., Chaabouni, H., Berson, E.L., and Hejtmancik, J.F. (2011). Molecular analysis of Bardet-Biedl syndrome families: report of 21 novel mutations in 10 genes. Invest. Ophthalmol. Vis. Sci. *52*, 5317–5324.
47. Redin, C., Le Gras, S., Mhamdi, O., Geoffroy, V., Stoetzel, C., Vincent, M.C., Chiurazzi, P., Lacombe, D., Ouertani, I., Petit, F., et al. (2012). Targeted high-throughput sequencing for diagnosis of genetically heterogeneous diseases: efficient mutation detection in Bardet-Biedl and Alström syndromes. J. Med. Genet. *49*, 502–512.
48. Saunier, S., Calado, J., Benessy, F., Silbermann, F., Heilig, R., Weissenbach, J., and Antignac, C. (2000). Characterization of the NPHP1 locus: mutational mechanism involved in deletions in familial juvenile nephronophthisis. Am. J. Hum. Genet. *66*, 778–789.
49. Hildebrandt, F., Otto, E., Rensing, C., Nothwang, H.G., Vollmer, M., Adolphs, J., Hanusch, H., and Brandis, M.

(1997). A novel gene encoding an SH3 domain protein is mutated in nephronophthisis type 1. Nat. Genet. *17*, 149–153.

50. Caridi, G., Murer, L., Bellantuono, R., Sorino, P., Caringella, D.A., Gusmano, R., and Ghiggeri, G.M. (1998). Renal-retinal syndromes: association of retinal anomalies and recessive nephronophthisis in patients with homozygous deletion of the NPH1 locus. Am. J. Kidney Dis. *32*, 1059–1062.
51. Raychaudhuri, S., Iartchouk, O., Chin, K., Tan, P.L., Tai, A.K., Ripke, S., Gowrisankar, S., Vemuri, S., Montgomery, K., Yu, Y., et al. (2011). A rare penetrant mutation in CFH confers high risk of age-related macular degeneration. Nat. Genet. *43*, 1232–1236.
52. van de Ven, J.P., Nilsson, S.C., Tan, P.L., Buitendijk, G.H., Ristau, T., Mohlin, F.C., Nabuurs, S.B., Schoenmaker-Koller, F.E., Smailhodzic, D., Campochiaro, P.A., et al. (2013). A functional variant in the CFI gene confers a high risk of age-related macular degeneration. Nat. Genet. *45*, 813–817.
53. Carvalho, C.M., Zhang, F., Liu, P., Patel, A., Sahoo, T., Bacino, C.A., Shaw, C., Peacock, S., Pursley, A., Tavyev, Y.J., et al. (2009). Complex rearrangements in patients with duplications of MECP2 can occur by fork stalling and template switching. Hum. Mol. Genet. *18*, 2188–2203.
54. Zaghloul, N.A., Liu, Y., Gerdes, J.M., Gascue, C., Oh, E.C., Leitch, C.C., Bromberg, Y., Binkley, J., Leibel, R.L., Sidow, A., et al. (2010). Functional analyses of variants reveal a significant role for dominant negative and common alleles in oligogenic Bardet-Biedl syndrome. Proc. Natl. Acad. Sci. USA *107*, 10602–10607.
55. Jao, L.E., Wente, S.R., and Chen, W. (2013). Efficient multiplex biallelic zebrafish genome editing using a CRISPR nuclease system. Proc. Natl. Acad. Sci. USA *110*, 13904–13909.
56. Zhu, X., Xu, Y., Yu, S., Lu, L., Ding, M., Cheng, J., Song, G., Gao, X., Yao, L., Fan, D., et al. (2014). An efficient genotyping method for genome-modified animals and human cells generated with CRISPR/Cas9 system. Sci. Rep. *4*, 6420.
57. Drummond, I.A., and Davidson, A.J. (2010). Zebrafish kidney development. Methods Cell Biol. *100*, 233–260.
58. Boone, P.M., Yuan, B., Campbell, I.M., Scull, J.C., Withers, M.A., Baggett, B.C., Beck, C.R., Shaw, C.J., Stankiewicz, P., Moretti, P., et al. (2014). The Alu-rich genomic architecture of SPAST predisposes to diverse and functionally distinct disease-associated CNV alleles. Am. J. Hum. Genet. *95*, 143–161.
59. Boone, P.M., Liu, P., Zhang, F., Carvalho, C.M., Towne, C.F., Batish, S.D., and Lupski, J.R. (2011). Alu-specific microhomology-mediated deletion of the final exon of SPAST in three unrelated subjects with hereditary spastic paraplegia. Genet. Med. *13*, 582–592.
60. Verdin, H., D'haene, B., Beysen, D., Novikova, Y., Menten, B., Sante, T., Lapunzina, P., Nevado, J., Carvalho, C.M., Lupski, J.R., and De Baere, E. (2013). Microhomology-mediated mechanisms underlie non-recurrent disease-causing microdeletions of the FOXL2 gene or its regulatory domain. PLoS Genet. *9*, e1003358.
61. Stankiewicz, P., Sen, P., Bhatt, S.S., Storer, M., Xia, Z., Bejjani, B.A., Ou, Z., Wiszniewska, J., Driscoll, D.J., Maisenbacher, M.K., et al. (2009). Genomic and genic deletions of the FOX gene cluster on 16q24.1 and inactivating mutations of FOXF1 cause alveolar capillary dysplasia and other malformations. Am. J. Hum. Genet. *84*, 780–791.
62. Shlien, A., Baskin, B., Achatz, M.I., Stavropoulos, D.J., Nichols, K.E., Hudgins, L., Morel, C.F., Adam, M.P., Zhukova, N., Rotin, L., et al. (2010). A common molecular mechanism underlies two phenotypically distinct 17p13.1 microdeletion syndromes. Am. J. Hum. Genet. *87*, 631–642.
63. Carvalho, C.M., Pehlivan, D., Ramocki, M.B., Fang, P., Alleva, B., Franco, L.M., Belmont, J.W., Hastings, P.J., and Lupski, J.R. (2013). Replicative mechanisms for CNV formation are error prone. Nat. Genet. *45*, 1319–1326.
64. Gu, S., Yuan, B., Campbell, I.M., Beck, C.R., Carvalho, C.M., Nagamani, S.C., Erez, A., Patel, A., Bacino, C.A., Shaw, C.A., et al. (2015). Alu-mediated diverse and complex pathogenic copy-number variants within human chromosome 17 at p13.3. Hum. Mol. Genet. *24*, 4061–4077.
65. Hastings, P.J., Lupski, J.R., Rosenberg, S.M., and Ira, G. (2009). Mechanisms of change in gene copy number. Nat. Rev. Genet. *10*, 551–564.
66. McVey, M., and Lee, S.E. (2008). MMEJ repair of double-strand breaks (director's cut): deleted sequences and alternative endings. Trends Genet. *24*, 529–538.
67. Wang, K., Li, M., Hadley, D., Liu, R., Glessner, J., Grant, S.F., Hakonarson, H., and Bucan, M. (2007). PennCNV: an integrated hidden Markov model designed for high-resolution copy number variation detection in whole-genome SNP genotyping data. Genome Res. *17*, 1665–1674.
68. Kim, J.C., Badano, J.L., Sibold, S., Esmail, M.A., Hill, J., Hoskins, B.E., Leitch, C.C., Venner, K., Ansley, S.J., Ross, A.J., et al. (2004). The Bardet-Biedl protein BBS4 targets cargo to the pericentriolar region and is required for microtubule anchoring and cell cycle progression. Nat. Genet. *36*, 462–470.
69. Roa, B.B., Garcia, C.A., Pentao, L., Killian, J.M., Trask, B.J., Suter, U., Snipes, G.J., Ortiz-Lopez, R., Shooter, E.M., Patel, P.I., and Lupski, J.R. (1993). Evidence for a recessive PMP22 point mutation in Charcot-Marie-Tooth disease type 1A. Nat. Genet. *5*, 189–194.
70. Yang, Y., Muzny, D.M., Xia, F., Niu, Z., Person, R., Ding, Y., Ward, P., Braxton, A., Wang, M., Buhay, C., et al. (2014). Molecular findings among patients referred for clinical whole-exome sequencing. JAMA *312*, 1870–1879.
71. Stray-Pedersen, A., Backe, P.H., Sorte, H.S., Mørkrid, L., Chokshi, N.Y., Erichsen, H.C., Gambin, T., Elgstøen, K.B., Bjørås, M., Wlodarski, M.W., et al.; Baylor-Johns Hopkins Center for Mendelian Genomics (2014). PGM3 mutations cause a congenital disorder of glycosylation with severe immunodeficiency and skeletal dysplasia. Am. J. Hum. Genet. *95*, 96–107.
72. Bayer, D.K., Martinez, C.A., Sorte, H.S., Forbes, L.R., Demmler-Harrison, G.J., Hanson, I.C., Pearson, N.M., Noroski, L.M., Zaki, S.R., Bellini, W.J., et al. (2014). Vaccine-associated varicella and rubella infections in severe combined immunodeficiency with isolated CD4 lymphocytopenia and mutations in IL7R detected by tandem whole exome sequencing and chromosomal microarray. Clin. Exp. Immunol. *178*, 459–469.
73. Janssen, S., Ramaswami, G., Davis, E.E., Hurd, T., Airik, R., Kasanuki, J.M., Van Der Kraak, L., Allen, S.J., Beales, P.L., Katsanis, N., et al. (2011). Mutation analysis in Bardet-Biedl syndrome by DNA pooling and massively parallel resequencing in 105 individuals. Hum. Genet. *129*, 79–90.
74. Beales, P.L., Badano, J.L., Ross, A.J., Ansley, S.J., Hoskins, B.E., Kirsten, B., Mein, C.A., Froguel, P., Scambler, P.J., Lewis, R.A., et al. (2003). Genetic interaction of BBS1 mutations with alleles at other BBS loci can result in non-Mendelian Bardet-Biedl syndrome. Am. J. Hum. Genet. *72*, 1187–1199.

75. Davis, R.E., Swiderski, R.E., Rahmouni, K., Nishimura, D.Y., Mullins, R.F., Agassandian, K., Philp, A.R., Searby, C.C., Andrews, M.P., Thompson, S., et al. (2007). A knockin mouse model of the Bardet-Biedl syndrome 1 M390R mutation has cilia defects, ventriculomegaly, retinopathy, and obesity. Proc. Natl. Acad. Sci. USA *104*, 19422–19427.
76. Bhogaraju, S., Cajanek, L., Fort, C., Blisnick, T., Weber, K., Taschner, M., Mizuno, N., Lamla, S., Bastin, P., Nigg, E.A., and Lorentzen, E. (2013). Molecular basis of tubulin transport within the cilium by IFT74 and IFT81. Science *341*, 1009–1012.
77. Lucker, B.F., Behal, R.H., Qin, H., Siron, L.C., Taggart, W.D., Rosenbaum, J.L., and Cole, D.G. (2005). Characterization of the intraflagellar transport complex B core: direct interaction of the IFT81 and IFT74/72 subunits. J. Biol. Chem. *280*, 27688–27696.
78. Huangfu, D., Liu, A., Rakeman, A.S., Murcia, N.S., Niswander, L., and Anderson, K.V. (2003). Hedgehog signalling in the mouse requires intraflagellar transport proteins. Nature *426*, 83–87.
79. Niederriter, A.R., Davis, E.E., Golzio, C., Oh, E.C., Tsai, I.C., and Katsanis, N. (2013). In vivo modeling of the morbid human genome using *Danio rerio*. J. Vis. Exp. *78*, e50338.
80. McIntyre, J.C., Davis, E.E., Joiner, A., Williams, C.L., Tsai, I.C., Jenkins, P.M., McEwen, D.P., Zhang, L., Escobado, J., Thomas, S., et al.; NISC Comparative Sequencing Program (2012). Gene therapy rescues cilia defects and restores olfactory function in a mammalian ciliopathy model. Nat. Med. *18*, 1423–1428.
81. Bizet, A.A., Becker-Heck, A., Ryan, R., Weber, K., Filhol, E., Krug, P., Halbritter, J., Delous, M., Lasbennes, M.C., Linghu, B., et al. (2015). Mutations in TRAF3IP1/IFT54 reveal a new role for IFT proteins in microtubule stabilization. Nat. Commun. *6*, 8666.
82. Lee, M.S., Hwang, K.S., Oh, H.W., Ji-Ae, K., Kim, H.T., Cho, H.S., Lee, J.J., Yeong Ko, J., Choi, J.H., Jeong, Y.M., et al. (2015). IFT46 plays an essential role in cilia development. Dev. Biol. *400*, 248–257.
83. Kramer-Zucker, A.G., Olale, F., Haycraft, C.J., Yoder, B.K., Schier, A.F., and Drummond, I.A. (2005). Cilia-driven fluid flow in the zebrafish pronephros, brain and Kupffer's vesicle is required for normal organogenesis. Development *132*, 1907–1921.
84. Putoux, A., Thomas, S., Coene, K.L., Davis, E.E., Alanay, Y., Ogur, G., Uz, E., Buzas, D., Gomes, C., Patrier, S., et al. (2011). KIF7 mutations cause fetal hydrolethalus and acrocallosal syndromes. Nat. Genet. *43*, 601–606.
85. Zhang, Y., Seo, S., Bhattarai, S., Bugge, K., Searby, C.C., Zhang, Q., Drack, A.V., Stone, E.M., and Sheffield, V.C. (2014). BBS mutations modify phenotypic expression of CEP290-related ciliopathies. Hum. Mol. Genet. *23*, 40–51.
86. Hjeij, R., Lindstrand, A., Francis, R., Zariwala, M.A., Liu, X., Li, Y., Damerla, R., Dougherty, G.W., Abouhamed, M., Olbrich, H., et al. (2013). ARMC4 mutations cause primary ciliary dyskinesia with randomization of left/right body asymmetry. Am. J. Hum. Genet. *93*, 357–367.
87. Beales, P.L., Bland, E., Tobin, J.L., Bacchelli, C., Tuysuz, B., Hill, J., Rix, S., Pearson, C.G., Kai, M., Hartley, J., et al. (2007). IFT80, which encodes a conserved intraflagellar transport protein, is mutated in Jeune asphyxiating thoracic dystrophy. Nat. Genet. *39*, 727–729.
88. Halbritter, J., Bizet, A.A., Schmidts, M., Porath, J.D., Braun, D.A., Gee, H.Y., McInerney-Leo, A.M., Krug, P., Filhol, E., Davis, E.E., et al.; UK10K Consortium (2013). Defects in the IFT-B component IFT172 cause Jeune and Mainzer-Saldino syndromes in humans. Am. J. Hum. Genet. *93*, 915–925.
89. Fromer, M., Moran, J.L., Chambert, K., Banks, E., Bergen, S.E., Ruderfer, D.M., Handsaker, R.E., McCarroll, S.A., O'Donovan, M.C., Owen, M.J., et al. (2012). Discovery and statistical genotyping of copy-number variation from whole-exome sequencing depth. Am. J. Hum. Genet. *91*, 597–607.
90. Krumm, N., Sudmant, P.H., Ko, A., O'Roak, B.J., Malig, M., Coe, B.P., Quinlan, A.R., Nickerson, D.A., and Eichler, E.E.; NHLBI Exome Sequencing Project (2012). Copy number variation detection and genotyping from exome sequence data. Genome Res. *22*, 1525–1532.
91. Katsanis, S.H., and Katsanis, N. (2013). Molecular genetic testing and the future of clinical genomics. Nat. Rev. Genet. *14*, 415–426.